

2011

Performance of twin-rotor DC homopolar motor

Zhiwei Wang

Louisiana State University and Agricultural and Mechanical College, zwang22@lsu.edu

Follow this and additional works at: https://digitalcommons.lsu.edu/gradschool_theses



Part of the [Electrical and Computer Engineering Commons](#)

Recommended Citation

Wang, Zhiwei, "Performance of twin-rotor DC homopolar motor" (2011). *LSU Master's Theses*. 1136.
https://digitalcommons.lsu.edu/gradschool_theses/1136

This Thesis is brought to you for free and open access by the Graduate School at LSU Digital Commons. It has been accepted for inclusion in LSU Master's Theses by an authorized graduate school editor of LSU Digital Commons. For more information, please contact gradetd@lsu.edu.

PERFORMANCE OF TWIN-ROTOR DC HOMOPOLAR MOTOR

A Thesis

**Submitted to the Graduate Faculty of the
Louisiana State University and
Agricultural and Mechanical College
in partial fulfillment of the
requirements for the degree of
Master of Science in Electrical Engineering**

in

The Department of Electrical & Computer Engineering

by

Zhiwei Wang

Bachelor of Engineering, Taiyuan University of Technology, 2004

Master of Engineering, McNeese State University, 2008

May 2011

Dedicated to my dearest parents

ACKNOWLEDGEMENTS

I would like to express my gratitude to my advisor, Dr. Ernest A. Mendrela, for his invaluable suggestions and constant patience in guiding me throughout the research. His technical advice and expertise in the field provided me the motivation towards successful completion of this thesis.

Also, I would like to thank the members of my committee, Dr. Kemin Zhou and Dr. Shahab Mehraeen, for sparing time out of their busy schedule and providing valuable suggestions.

I would like to thanks to my parents, who have always trusted me and support me to study here to realize my dreams. Thousands words cannot express how thankful I am to them for their love and support. I would like to my colleague, Pavani Gottipati and Alex, who give me useful support and encourage me. I deeply appreciate your time and help.

Last, I hope this thesis will be on step leading me to become a professional engineer.

TABLE OF CONTENTS

ACKNOWLEDGEMENTS.....	iii
LIST OF TABLES.....	vi
LIST OF FIGURES.....	vii
ABSTRACT.....	ix
CHAPTER 1 INTRODUCTION.....	1
1.1 History and Literature Review on DC Homopolar Motors.....	1
1.2 Objectives of the Thesis.....	6
1.3 Thesis Outline.....	6
CHAPTER 2 MODELING MOTOR IN 3-D FEM.....	8
2.1 Basic Maxwell Equations for Electric Motors.....	8
2.2 Description of MAXWELL 12v Program.....	9
2.2.1 Drawing and Setting Tools.....	10
2.2.2 Postprocessor Mode.....	13
2.3 Why to Build Model in 3-D, not in 2-D.....	15
CHAPTER 3 DESIGN PARAMETERS OF TWIN-ROTOR DC HOMOPOLAR DISC MOTOR.....	16
CHAPTER 4 DETERMINATION OF ELECTROMECHANICAL PARAMETERS OF THE MOTOR.....	22
4.1 Motor Model in 3D FEM MAXWELL.....	22
4.2 Currents Density Distribution in Aluminum Discs.....	23
4.3 Magnetic Flux Density Distribution in the Motor.....	24
4.4 Electromagnetic Forces and Torque in the Motor.....	26
4.4.1 Provisional Torque Calculation.....	26
4.4.2 Forces and Torque Determination using FEM.....	26
4.4.3 Discussion on Discrepancies between Rouge Assessment and FEM Results...27	
4.5 Determination Parameters of the Motor Equivalent Circuit Parameters.....	29
4.6 Parameters of Equivalent Mechanical System.....	33
CHAPTER 5 MOTOR PERFORMANCE IN STEADY-STATE AND DYNAMIC CONDITIONS.....	36
5.1 Motor Performance in Steady-State Condition.....	36

5.2 Analysis of Motor Performance in Dynamic Conditions.....	39
5.3 Verification of Simulation Results.....	44
CHAPTER 6 CONCLUSIONS AND FUTURE WORK.....	47
6.1 Conclusions of the Twin-Rotor Homopolar DC Motor.....	47
6.2 Future Work.....	48
REFERENCES.....	49
APPENDIX A: M-FILES FOR STEADY STATE CHARACTERISTICS OF TWIN-ROTOR HOMOPOLAR DC MOTOR.....	50
APPENDIX B: M-FILES FOR DYNAMIC CHARACTERISTICS OF TWIN-ROTOR HOMOPOLAR DC MOTOR.....	51
VITA.....	52

LIST OF TABLES

Table 2.1: Symbols and units of basic Maxwell equation.....	9
Table 3.1: Specifications for the disc type twin-rotor homopolar DC motor.....	19
Table 4.1: Aluminum discs and iron discs.....	34
Table 4.2: Parameters of electric equivalent circuit and mechanical system.....	35
Table 5.1: Electromechanical parameters.....	39

LIST OF FIGURES

Figure 1.1: Faraday’s disk generators.....	1
Figure 1.2: Principle of homopolar motor operation.....	1
Figure 1.3: Homopolar DC motor with axial flux.....	2
Figure 1.4: Another structure of homopolar DC motor.....	4
Figure 1.5: Longitudinal section of DC homopolar motor applied to drive the ship by General Atomics Company.....	5
Figure 1.6: New concept of marine propulsion system with dual-rotor machine.....	5
Figure 2.1: Drawing mode toolbar buttons.....	10
Figure 2.2: Modelor mode toolbar.....	10
Figure 2.3: View toolbar buttons.....	11
Figure 2.4: Editing toolbar buttons of moving, duplicating, and mirroring.....	11
Figure 2.5: Assigning NdFe35 material parameters.....	12
Figure 2.6: Checking button function.....	14
Figure 3.1:Diagram of homopolar DC motor: F -electromagnetic force, I_a -armature current, ω_m -speed.....	17
Figure 3.2: Dimensions of the disc motor.....	18
Figure 3.3: Magnetization characteristic: (a) stator core, (b) rotor core.....	19
Figure 3.4: The middle radius R_{av}	21
Figure 4.1: Twin-Rotor homopolar DC motor model.....	22
Figure 4.2: The distribution of current density in the aluminum discs.....	23
Figure 4.3: Ohmic power losses distribution in the discs.....	24
Figure 4.4: Magnetic flux density distributions in the motor.....	25
Figure 4.5: Magnetic flux distributions on the aluminum discs.....	27

Figure 4.6: One specified part of the current flux density distribution.....	28
Figure 4.7: Left-hand and right-hand symmetrical current flowing paths.....	29
Figure 4.8: Explanation of equation (4.10).....	30
Figure 4.9: Aluminum disc shown in form of aluminum bars.....	31
Figure 4.10: FEM model for inductance determination.....	32
Figure 5.1: The motor equivalent circuit in steady-state.....	36
Figure 5.2: Characteristics of angular speed and armature current vs. load torque on shaft...38	
Figure 5.3: Characteristics of input power, out power and efficiency vs. load torque on shaft.....	38
Figure 5.4: Equivalent circuit of homopolar DC motor for dynamic analysis.....	39
Figure 5.5: Mechanical equivalent system of homopolar motor.....	40
Figure 5.6: Block diagram of homopolar DC motor.....	41
Figure 5.7: Simulink block diagram of homopolar DC motor for analysis in dynamic condition.....	41
Figure 5.8: Angular speed, electromagnetic torque, load torque waveforms.....	42
Figure 5.9: Armature current vs. time characteristics.....	42
Figure 5.10: Current, supply voltage and speed characteristic with ramped start-up.....	43
Figure 5.11: Block diagram for ramped start-up.....	43
Figure 5.12: The real model of twin-rotor homopolar DC motor in LSU Power Lab.....	44
Figure 5.13: Scheme of the PM homopolar motor with the aluminum disc mounted to the stator (M-point of measurement).....	45
Figure 5.14: flux density distribution in radial direction in femm software.....	46
Figure 5.15 Femm software model of the motor with aluminum discs on the stator.....	46

ABSTRACT

A new concept of dual-rotor motor with counter-rotating propeller increases the efficiency of the ship propulsion used in marine industry. This concept can be realized by twin-rotor permanent magnet homopolar disc motor, which is the object of this thesis.

The objectives of this thesis are to determine the motor electromechanical parameters applying a 3-D FEM modeling and to analyze the motor performance in steady-state and dynamic conditions.

The objectives of this thesis are to determine the PM DC homopolar twin-rotor disc motor electromechanical parameters by 3-D FEM modeling. Furthermore, the PM DC Homopolar perform determination in steady-state and dynamic conditions. To reach these objectives, a 3-D model of the twin-rotor type of homopolar PM DC motor is developed using Ansoft Maxwell V12 software package. From modeling the motor magnetic flux and current flow density distribution on the aluminum disc and the electromechanical parameters were determined. Next, applying the electric equivalent circuit and mechanical equivalent system, the steady-state model and dynamic motor mode was developed in Matlab/Simulink software and the performance of the homopolar motor was analyzed.

From the analysis, the following conclusions were deduced:

- To produce the relatively high electromagnetic torque a very high currents have to be supplied to the rotor aluminum discs what is the major deficiency of the motor
- The currents are distributed non-uniformly in the disc what makes the electromagnetic torque smaller. To improve this, more brushes should be applied

around the disc periphery.

- The proposed construction of the motor allows one rotor disc to rotate in direction opposite to the rotation of other rotor disc. This can be done by reversing the current flow in one of the aluminum discs.

CHAPTER 1 INTRODUCTION

1.1 History and Literature Review on DC Homopolar Motors

Michael Faraday was the first who built and demonstrated electromagnetic rotation experiment in 1821 at the Royal Institution in London. This type of motor was the first device which produced rotation from electromagnetism itself [1]. The concept of homopolar generator (see figure 1.1) is the first DC electrical generator developed by Michael Faraday in 1831.

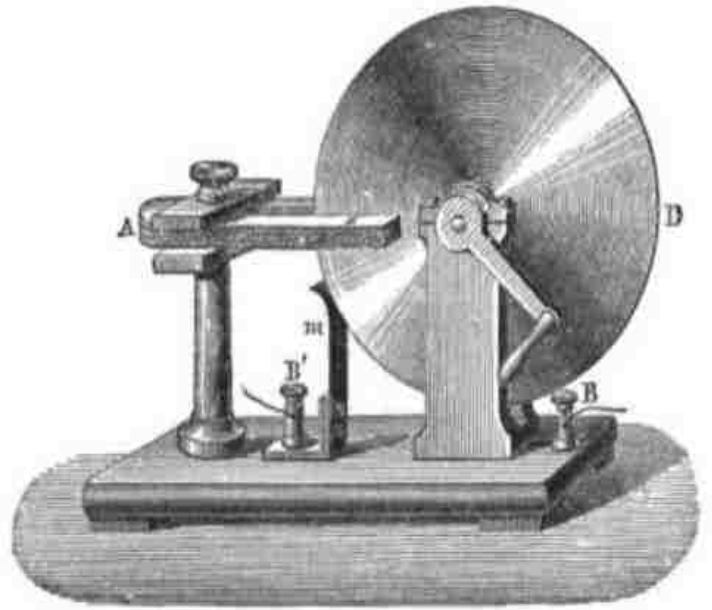


Figure 1.1 Faraday's disk generators [2]

The figure 1.2 illustrates the principle of operation of the Faraday's disc working as a motor. The disc made of aluminum or copper is placed in the air-gap of the electromagnet.

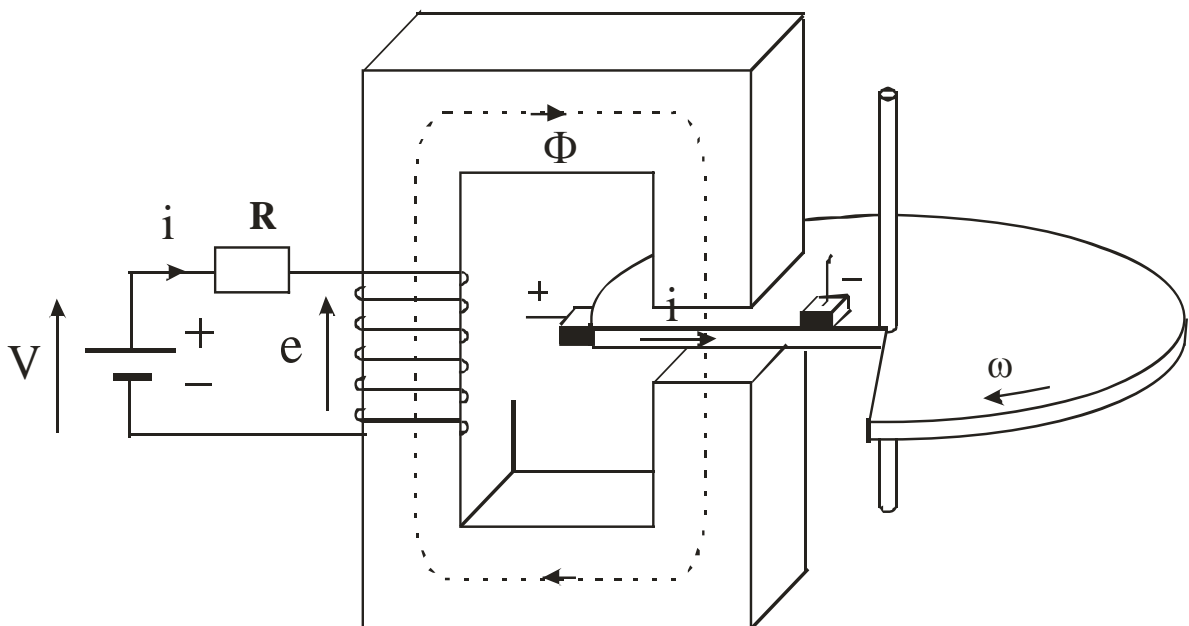


Figure 1.2 Principle of homopolar motor operation [3]

The disc is supplied by DC current through brushes. The interaction of disc current and magnetic field generated by the electromagnet gives rise to the electromagnetic torque that drives the disc. The major deficiency of this type of motor is the high current which supplies the disc necessary to produce torque. The great advantage of the motor is the lack of commutator that is in DC motors. The negative feature mentioned above makes this motor not very popular.

On the basis of the Faraday's disc, several other structures of the homopolar motors were proposed. One of them is shown in figure 1.3.

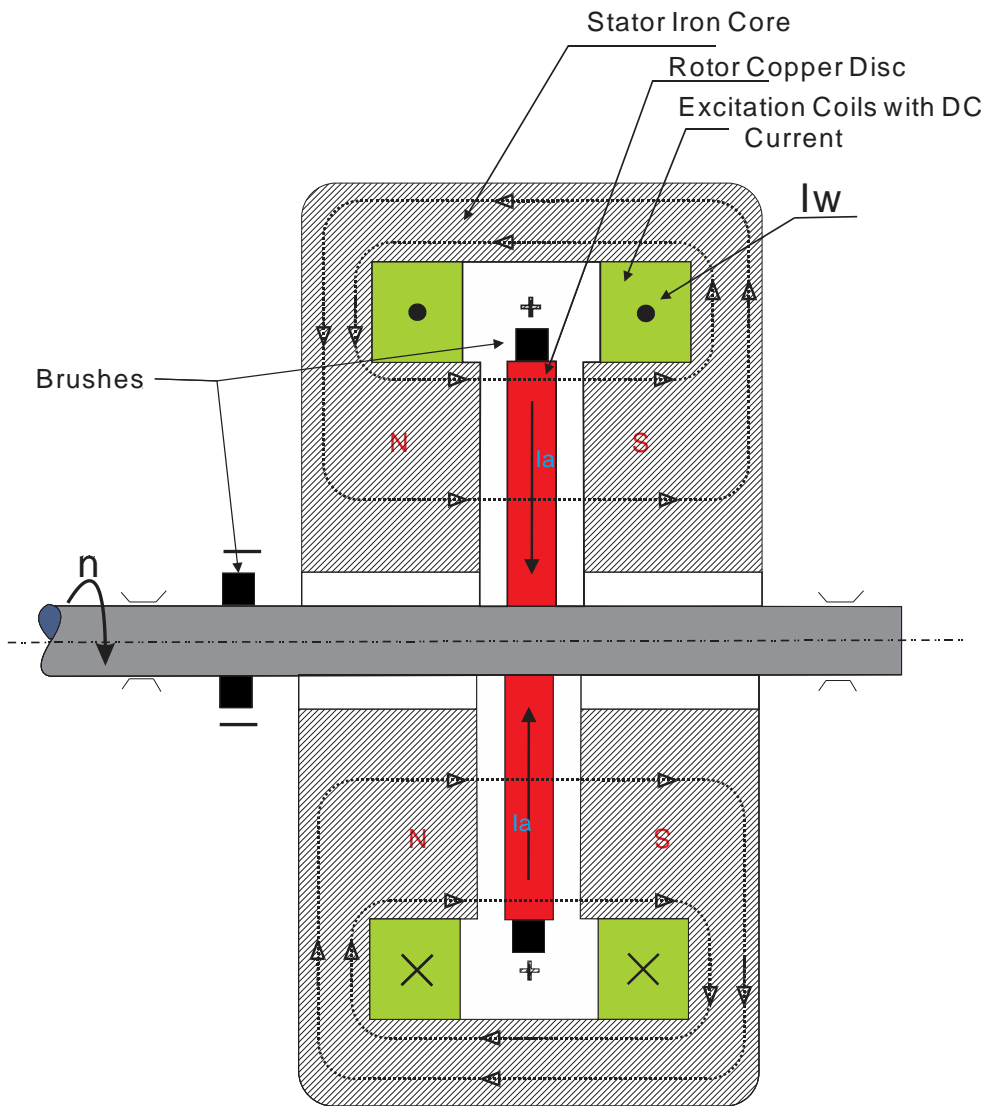


Figure 1.3 Homopolar DC motor with axial flux

The stator consists of iron core and two excitation coils. The rotor in a form of copper disc is placed in the gap between two stator magnetic poles. The excitation coils are supplied by DC current, which generates the magnetic flux, which goes throughout the rotor disc in axial direction. The rotor disc is supplied by DC current through the brushes of which one set of brushes touching the disc at its periphery has positive polarity and the other, touching the rotor shaft has negative polarity.

The current that flows through the disc interact with magnetic field around the whole circumference producing the torque that drives the rotor. The direction of rotation depends on the polarity of the DC voltage across the brushes.

Another homopolar machine is shown in figure 1.4. The stator is in a form of ferromagnetic cylinder with two coils. The rotor consists of ferromagnetic core attached to the shaft and a copper cage. The cage has the bar placed axially in the core and are short circuited by the rings at both sides.

The stator coils are excited by the DC current flowing in opposite directions with respect to one another. This current generates the magnetic flux that passes to the rotor through the air-gap in radial direction. The rotor rings are supplied through the brushes that are distributed uniformly around each ring. The currents that flow through the bars embedded in the rotor core interact with the magnetic flux giving the torque that drives the rotor.

Despite the deficiency the homopolar DC motors suffer there are various applications of these motors. One of them is propulsion of the ship. The company of General Atomics claims that has developed and demonstrated the reliability of conduction cooled SC systems for full-scale homopolar motors for the U.S. Navy under high shock and vibration environment.

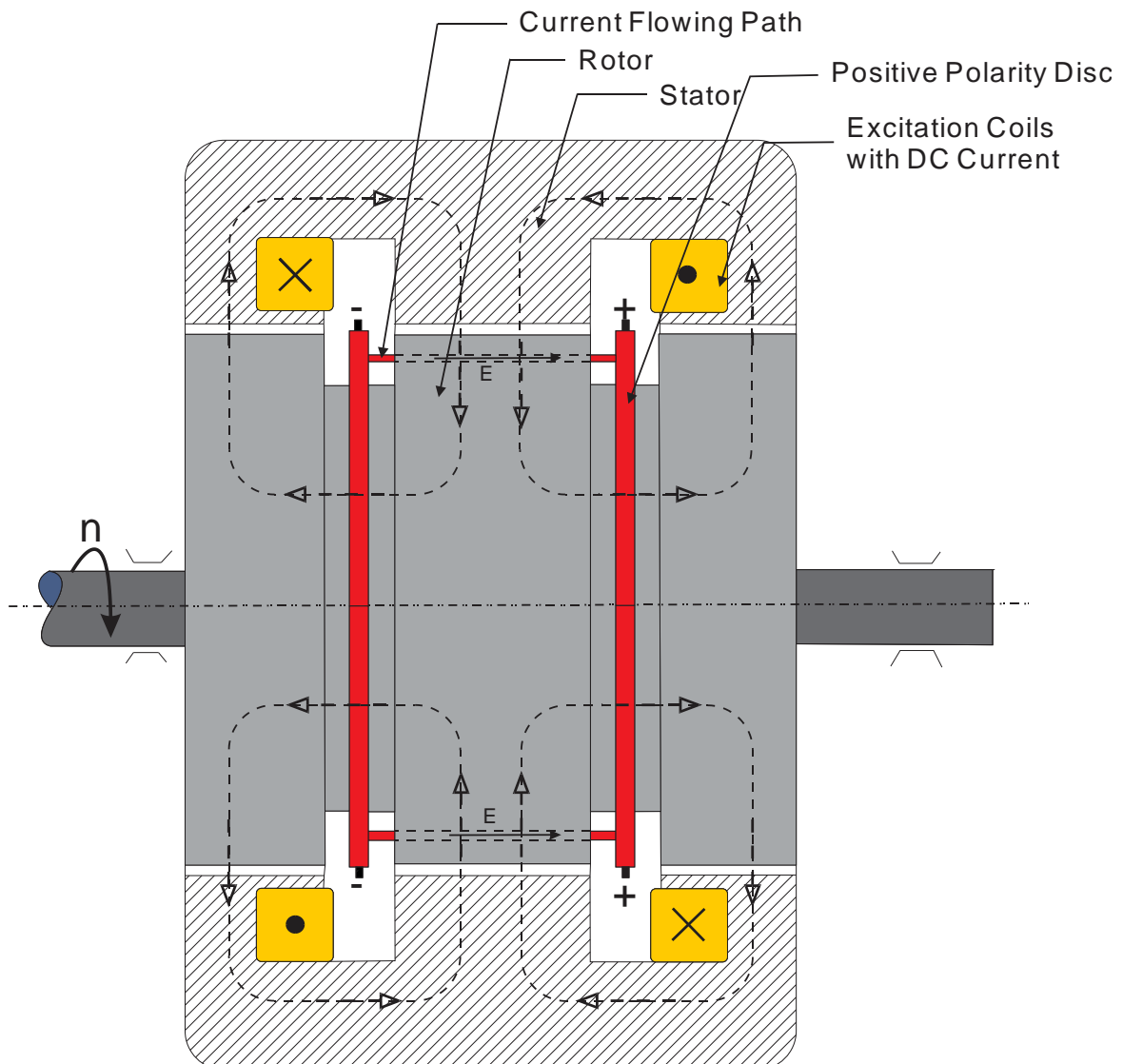


Figure 1.4 Another structure of homopolar DC motor

The basic structure is as shown in figure 1.5. A copper or aluminum disc rotates between U-shaped PM poles. One set of brushes collect the current from the shaft and the second brush set is placed close to the outer diameter of the disc. At the corner of the motor, there are two sets of DC field excitation coils generate magnetic flux. The magnetic flux interact with currents flows on the discs to make the effective electromagnetic torque which push the shaft rotating. [4]

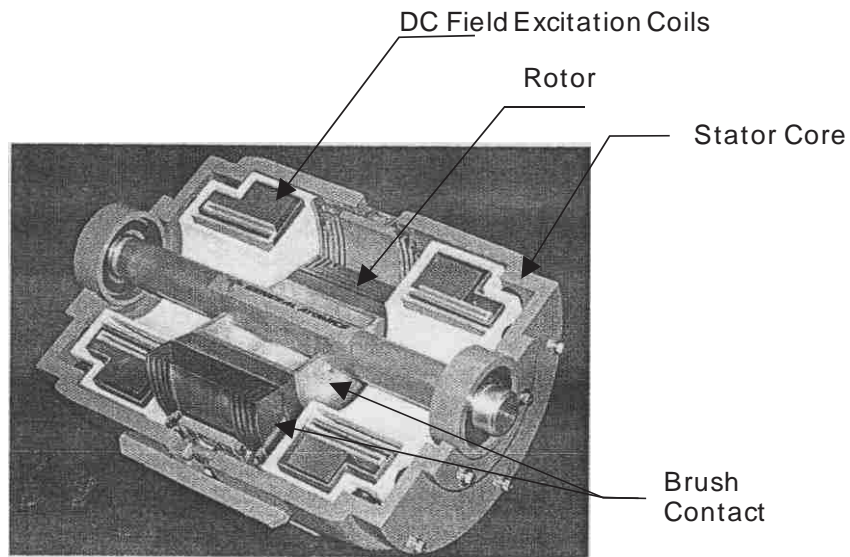


Figure 1.5 Longitudinal section of DC homopolar motor applied to drive the ship by General Atomics Company [4]

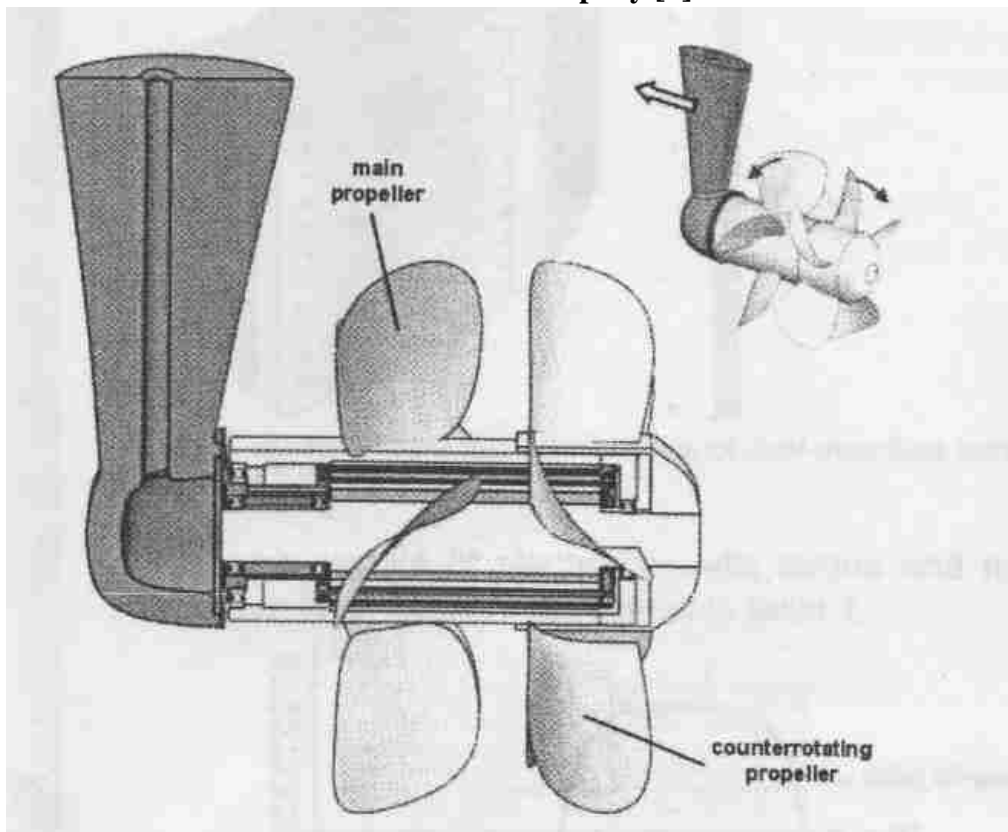


Figure 1.6 New concept of marine propulsion system with dual-rotor machine [5]

Referring to the ship propulsion, a new concept of marine propulsion system with dual-rotor machine is shown in figure 1.6. A dual-rotor type motor having counter-rotating propeller increase the water flowing efficiency. [5]

The concept of counter-rotating propulsion and the idea at homopolar DC motor are the basis for PM DC homopolar twin-rotor disc motor, which is the subject at this thesis project.

1.2 Objectives of the Thesis

The objectives of this thesis are:

- Determination of the PM DC homopolar twin-rotor disc motor electromechanical parameters by 3-D FEM modeling.
- PM DC homopolar motor performance determination in steady-state and dynamic conditions.

The tasks to accomplish the thesis project are as follows:

- Developing a 3-D model of the disc-type and homopolar PM twin-disc motor using the software package Ansoft Maxwell V12.
- Determining the motor magnetic flux and current flow density distribution on the aluminum disc plate and the electromechanical parameters of the motor using the software package Ansoft MAXWELL V12.
- Development of steady-state model of the motor and determination of motor performance.
- Simulation of motor dynamics using Matlab/Simulink DC motor model.

1.3 Thesis Outline

- Chapter 2 discusses basic Maxwell equations for the electric machine modeling and numerical methods to solve them. Description of MAXWELL 12V program is presented and explanation why was chosen 3D modeling instead of simple 2D modeling is given.

- Chapter 3 presents the twin-disc PM DC motor, with all design data.
- Chapter 4 provides the simulation model in MAXWELL 12v software in order to determine distribution of the magnetic flux in the motor and currents in the rotor discs. Also, the electromechanical parameters like electromotive force, torque, and stator resistance and inductance are obtained from the model.
- Chapter 5 shows a Matlab/Simulink model for analysis of the motor performance in dynamic conditions. Also, circuit model of the motor in steady-state is presented and analysis of the motor characteristics is done.
- Chapter 6 concludes the results obtained, compares the results got from calculations with the test results and points to the future research.

CHAPTER 2 MODELING MOTOR IN 3-D FEM

Computer-aided software is very widely used in engineering tasks. In electric machine designing a finite element method (FEM) is applied to optimize the construction. FEM has several packages which can help shortening development period before the real model is built. The MAXWELL is one of the advanced software of Ansoft Group to solve the electromagnetic problems. It allows solving numerically the Maxwell's differential field equations.

2.1 Basic Maxwell Equations for Electric Motors:

The basic Maxwell equations are:

Ampere's Law

$$\nabla \times H = J \quad (2.1)$$

Gauss's Law for magnetism

$$\nabla \cdot B = 0 \quad (2.2)$$

Maxwell-Faraday equation

$$\nabla \times E = -\frac{\alpha B}{\alpha t} \quad (2.3)$$

And the relation between magnetic field intensity and flux density is

$$B = \mu H \quad (2.4)$$

By Helmholtz's theorem, B can be written in terms of a vector potential A:

$$B = \nabla \times A \quad (2.5)$$

Hence, the equation (2.1) and (2.2) can be rewritten in terms of magnetic vector potential

A:

$$\nabla \times \left(\frac{\nabla \times A}{\mu} \right) = J \quad (2.6)$$

The symbols used in the equations above have meaning shown in Table 2.1.

Table 2.1 Symbols and units of basic Maxwell equations

Symbol	Meaning	Unit
E	Electric field intensity	Volt per meter
B	Magnetic field density	Tesla
H	Magnetic field intensity	Amperes per meter
J	Free current density	Amperes per square meter

When the model of the motor is built in 3-D, the Maxwell's equations can be solved either analytically or numerically. In case of electric machines where the structure is complex and a nonlinearity of magnetic circuit occur the numerical solution is applied. One of many numerical methods is a finite element method (FEM). This method has been used in this thesis applying the Maxwell 12v program of Ansoft Company.

2.2 Description of MAXWELL 12v Program [7]

Ansoft's Maxwell 12v software is one of advanced FEM tools to design, solve static, frequency-domain and time-varying electromagnetic and electric field problem. It allows to build and analyze 3-D and 2-D electromagnetic and electromechanical devices such as motors, actuators, transformers, sensors and coils.

For Maxwell 3D designs, the major solver types are:

- ◆ Magnetostatic
- ◆ Eddy current
- ◆ Transient
- ◆ Electrostatic
- ◆ DC conduction, either with or without insulator field

◆ Electric transient

2.2.1 Drawing and Setting Tools



- Drawing Tools

The Maxwell 3D object tools allows to draw one, two, three-dimensional objects as line, polyline, center-point arc line, rectangles, ellipses, circles, regular polygons, boxes, cylinders, regular polyhedrons, cones, spheres and helices. The general step is: first, click the button with the shape you want to create and set the starting point in coordinate X, Y, and Z. Then, type the coordinates of a point relative to the center point in the dX, dY and dZ box (see figure 2.1).



Figure 2.1: Drawing mode toolbar buttons

After the basic 3-D model is created, the splitting, separating, combining parts allows to match the original design shape. The designer can set up Boolean function using modeler menu (see figure 2.2). Also, the customer can size or move the view in 3D dimensions by using the view toolbar button shown in figure 2.3.

The buttons  can make a selected part to be invisible. When you click and hold  button, and move in four arrow directions, the model moves by

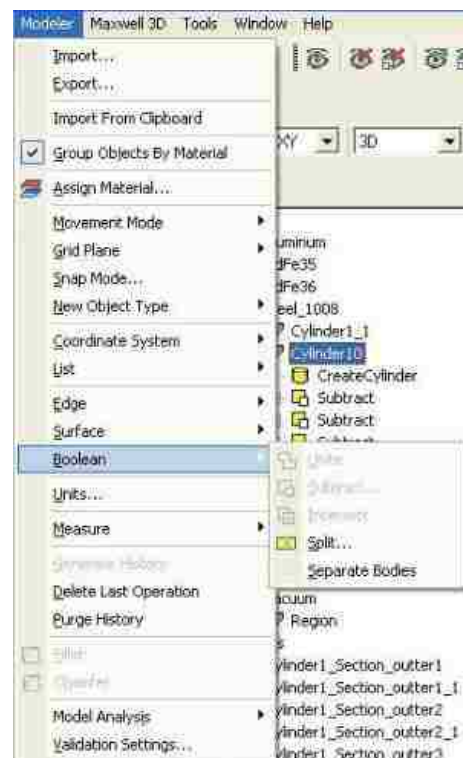


Figure 2.2 Modelor mode toolbar

a distance according to the mouse moving direction. When you click and hold  or 




button, and move in two freedom directions, the model will rotate in 3D dimensions along the holding point. The  button help you to adjust the model in 2D dimension. The buttons  help to zoom in and out the current view and buttons  help to resume original size of the model.



Figure 2.3 View toolbar buttons


As the initial parts of model geometry are created, you may need to modified model by the editing buttons. To resume last modification the “undo” buttons can help to do this. Also, if the design parts need moving, duplicating, mirroring by specified axis, the editing toolbar have these function and it is shown in figure 2.4.



Figure 2.4 Editing toolbar buttons of moving, duplicating, and mirroring

Maxwell 12v allows the user to create coordinate systems. There are 3 choices: global, relative, and face coordinate system. The user can choose one of them to match his original design.

- **Setting Tools**

When the geometry of the model is built, assigning materials for each part of the model is the next step for the simulation. The Maxwell 12v software gives a plenty of materials parameters for setting. First, select the geometry part and click button  . Then, in the

new box assign the material parameters. For example, when setting the NdFe 35 permanent magnet, user also needs to select the magnet flux type and direction of magnetization. If the material has some specified setting, clone the material and save as a new name for it (see figure 2.5).

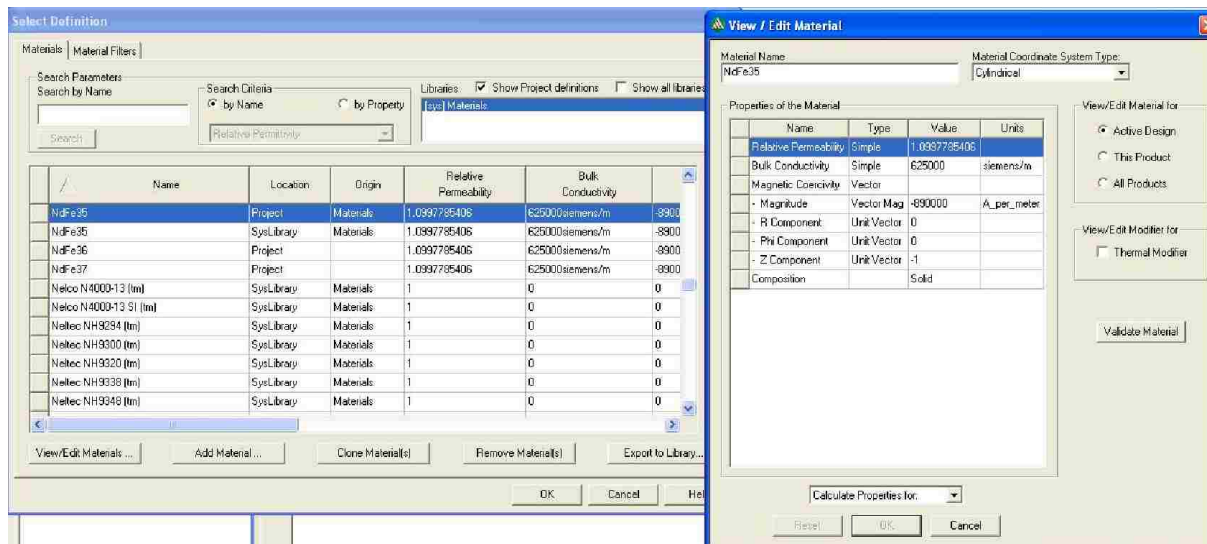


Figure 2.5 Assigning NdFe35 material parameters


For Boundary setting, Maxwell 12v allows the magnetostatic, electrostatic, DC conduction, eddy Current, 3D transient boundary condition to setup. Users can assign its insulating, symmetry, master, slave, zero tangential H field for each part to make the simulation more accurate.

Defining excitations is essential for the success simulation. User can assign voltage, voltage drop, current density, current density terminal, or current flow direction according to the design purpose. If setting current, current density terminals or coil terminals, be aware of assigning the flowing direction. After all, user needs to set the region of the model in order to make the Maxwell 12v software recognizing the geometry size of the model for simulation.

2.2.2 Postprocessor Mode

Like other FEM softwares, the Maxwell 12v can solve the force, torque and self inductance problem. To assign a force/torque parameter follows the step: select the object for which part you want to apply the parameter; click Maxwell 3D, then select parameters>assign>force/torque; type a name for the force/torque; select type force/torque you want to simulate; for torque, a user needs to assign an axis of the direction. The function of matrix setting is similar as torque set, but it requires the user to specify the sources which coil flowing paths want to count. When simulation is done, click the matrix button and the software shows the values of each inductance of the coil.

Maxwell 12v also gives a path for mesh refinement on the object faces, inside objects, and skin depth-base mesh refinement on object faces. The smaller is the element setting, the more accurate are calculation results, but it takes more time and may lead to computer memory error.

For magnetic problem, the Maxwell 12v gives several definitions which need to be assigned in the solution function: convergence, solver, general, and defaults. Because the convergence for different model has many setting, generally, set the maximum number of passes between 3 and 5 and 0.01 percent error. The more number of passes is specified, the more time takes the simulation. Checking the energy losses, error detection in each pass calculation is essential for the simulation results are correct or fake. After solution function setting of the model is done, pressing the  buttons is last step before simulation the model. They allow to check the model if each part setting is correct (see 2.6). Of course, if there has some problems the software will figure out which part needs to be fixed and give

suggestion links. User can refer these hints fixing the model and run check function again.

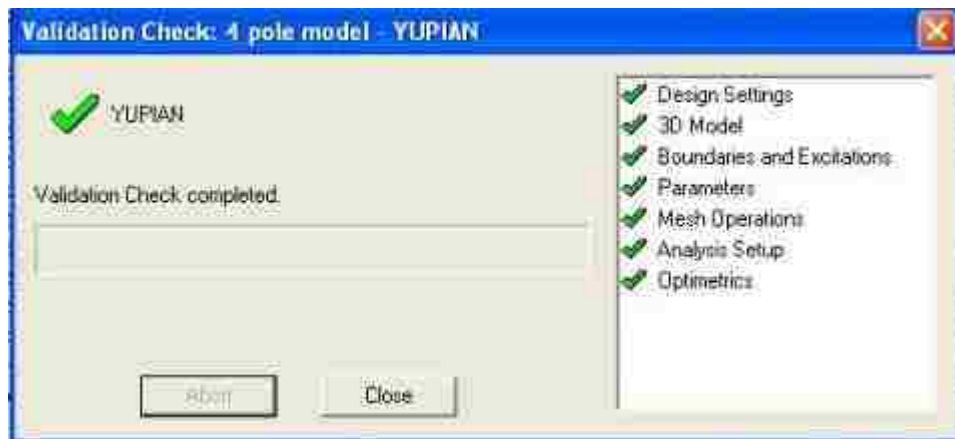




Figure 2.6 Checking button function

After simulation, the result mode can generate a graph, table, or 3D figure. The buttons  **Result** can create the report and  **Field Overlay** button can plot magnetic flux, current density distribution, magnetic flux density, and any energy flowing 3D figures. These functions can give users to arrange data and vivid figures which a user applies for further model analysis.

To summarize, there are following various steps in constructing and simulating a model and obtaining the results:

- 1) According to the defined problem definition and its specification, draw the model using 3D dimension tools: line, arc segments, rectangles, ellipses, circles and so on.
- 2) Assign to each part a solution region adding materials and define the properties of materials.
- 3) Assign the circuit properties to the model like voltage, current, or coil terminals.
- 4) Define and apply boundary conditions and assign mesh refinement.
- 5) Assign the magnetic solutions and specify related parameters; use checking function to detect model setting.

- 6) Analyze the problem and view results.
- 7) Plot the flux density figures in 3D which illustrate the results obtained and read various electromechanical parameters.

2.3 Why to Build Model in 3-D, not in 2-D

Any motor and generator in our real world have 3 dimensions properties and magnetic flux density also have 3 components of direction. The 3-D simulation can exactly illustrate the model performance in real world. Also, the analysis is more accurate if the model can be generated in 3-D. and simulating parameters will express more characteristics in dimensions.

Some of the machines cannot be modeled in 2-D. this concerns in particular all disc machines. The disc PM homopolar machine which is the object of the study was modeled in 2D using femm software in thesis on homopolar motor [10]. This required two models to be built to get accurate results, but still they are affected by the error caused by simplification in model geometry. The 3-D model can break this limitation and Ansoft Maxwell 12v with its powerful tools can fulfill this task. That is why the Maxwell v12 was chosen analyzing this motor instead of FEMM 4.0.

CHAPTER 3 DESIGN PARAMETERS OF TWIN-ROTOR DC HOMOPOLAR DISC MOTOR

The twin-rotor DC homopolar disc motor is shown schematically in the figure 3.1. The stator which is placed in the center of the motor consists of iron disc and two permanent magnets on its both sides. The PMs are magnetized axially, perpendicular to the disc surface as shown in figure 3.2. The rotor consists of two iron discs placed at the both sides of the stator. To the inner sides of the both iron discs, two aluminum discs are attached firmly. The aluminum discs are insulated from both rotor iron discs. There are inside of 4 pairs of brushes which are touching each aluminum discs and the brushes are supplied through wires from DC voltage source. The interaction of the currents which flow in the aluminum disc with the magnetic flux established in the air-gaps give rise to the electromagnetic torque. The direction of the torque acting on the rotor discs depends on polarity of the PMs and the direction of currents flowed in the aluminum discs. Changing the polarity of the supply voltage, the direction of the torque can be adjusted. With the polarity of magnets and voltages shown in figure 3.1, both rotor discs are driven by the torque in the opposite directions. For the polarity of the voltage as in parenthesis, the rotors are driven in the same directions. The dimensions of the motor are shown in figure 3.2. The parameters of the materials used in the disc motor and the assumed current density in the aluminum disc are shown in Table 3.1.

In simulation model developed in Maxwell 12 v, a current is assigned to the aluminum disc. Since the current density has been assumed of $J = 7 \text{ A/mm}^2$. it is necessary to find the rotor current that flows through the disc. To do it, a cross section area of the disc for the radius R_{av} at the middle needs to be determined as shown in figure 3.4

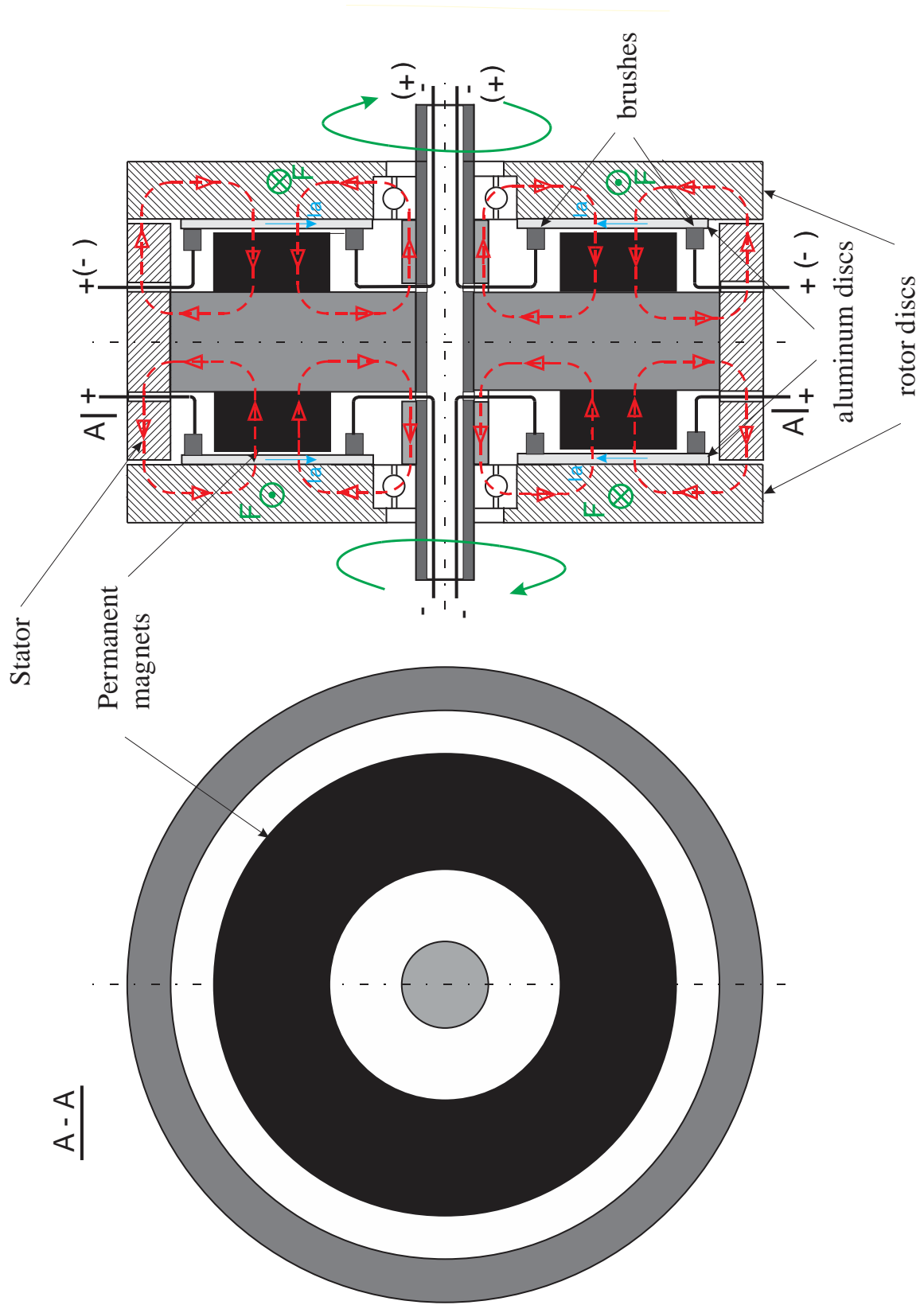


Figure 3.1 Diagram of homopolar DC motor: F - electromagnetic force, I_a - armature current, ω_m - speed

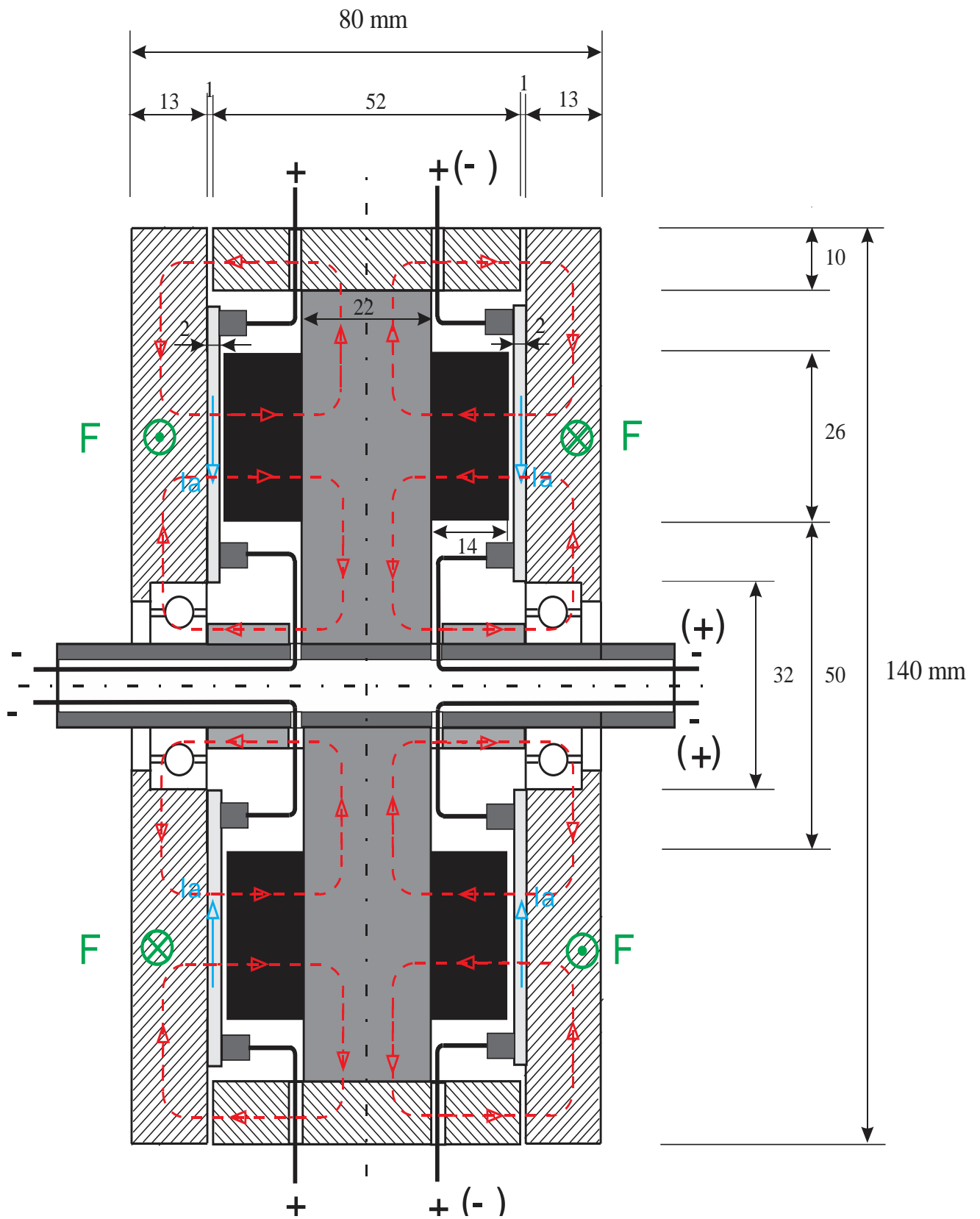
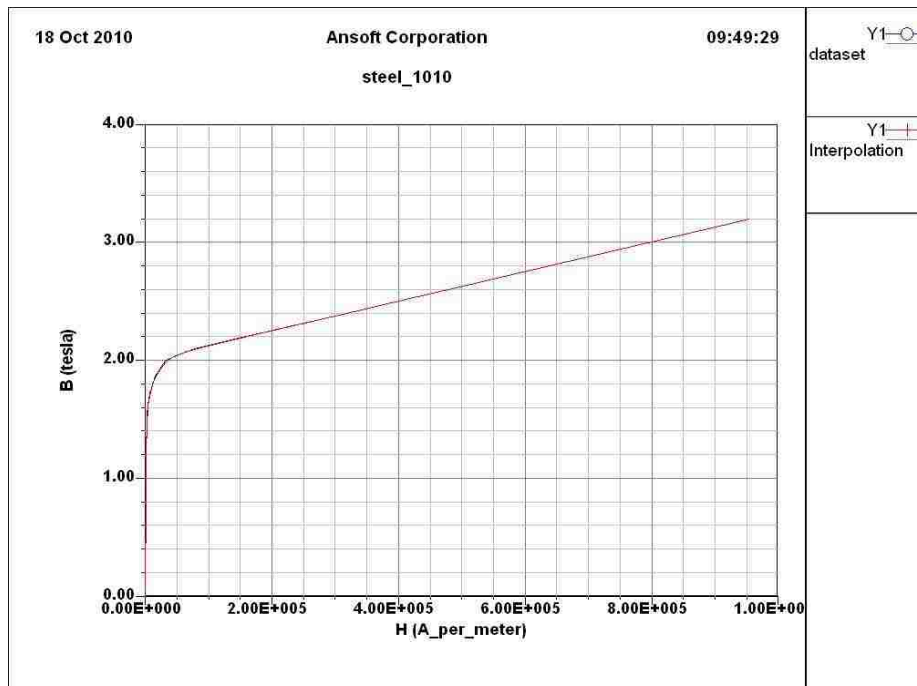


Figure 3.2 Dimensions of the disc motor

Table 3.1 Specifications for the disc type twin-rotor homopolar DC motor

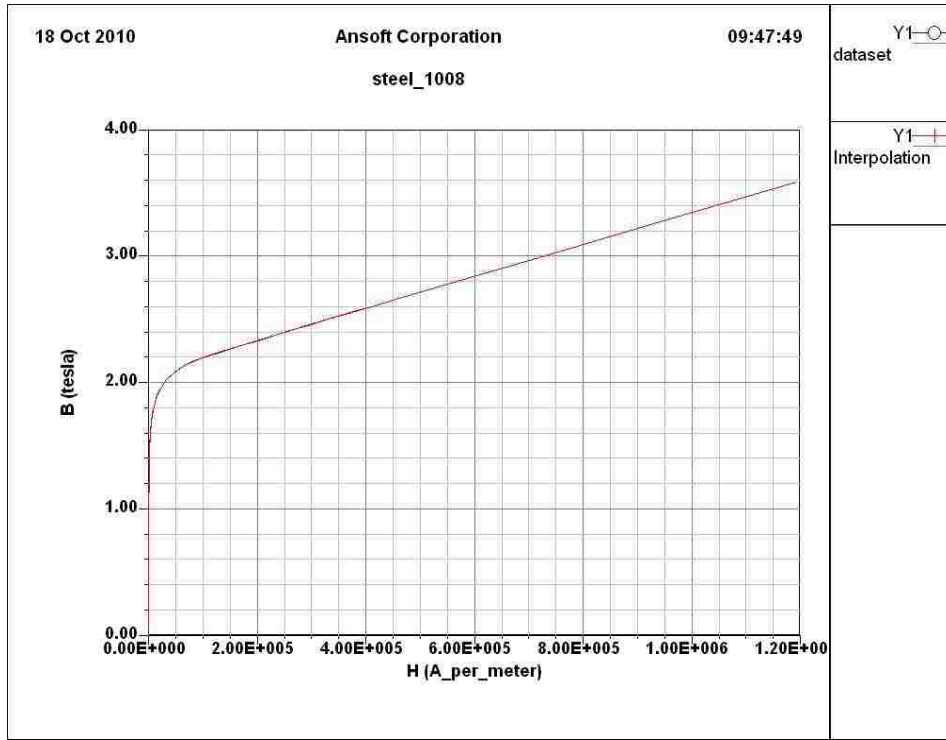
- Stator core	Solid steel with the B-H characteristic shown in figure 3.3a
- Rotor iron discs	Solid iron with the B-H characteristic shown in figure 3.3b
- Aluminum discs	Conductivity: 38,000,000 Siemens/m
- Permanent Magnets	NdFe35 $B_r = 1.230 T; H_c = 890,000 A/m$
- Magnet thickness	14 mm
- Shaft	Steel
- Supply wires	Copper: conductivity is 58,000,000 Siemens/m
Rotor speed	200 rad/s (1910 rpm)
4 pairs of brushes parameters	$2 \cdot 2 \cdot 5 \text{ mm}$ (wide · length · height)
Current density of the aluminum disc	$7 A/mm^2$



(a)

Figure 3.3: Magnetization characteristic: (a) stator core, (b) rotor core

(Figure 3.3 continued)



(b)

The inner radius of aluminum disc is $R_{inner} = 19 \text{ mm}$ and the outer radius of aluminum disc is $R_{outer} = 57 \text{ mm}$. The thickness of the aluminum disc is $d = 2 \text{ mm}$ (see figure 3.2)

Thus, the middle radius is:

$$R_{av} = \frac{R_{outer} - R_{inner}}{2} + R_{inner} = \frac{57 - 19}{2} + 19 = 38 \text{ mm} \quad (3.1)$$

The cross-section area in the middle of the disc is

$$A_{med} = 2\pi \cdot R_{av} \cdot d = 2\pi \cdot 0.038 \cdot 0.002 = 4.7752 \cdot 10^{-4} \text{ m}^2 = 477.52 \text{ mm}^2 \quad (3.2)$$

Hence, the total current that flows through on one disc is

$$I_a = J \cdot A_{med} = 7 \cdot 477.52 = 3344 \text{ A} \quad (3.3)$$

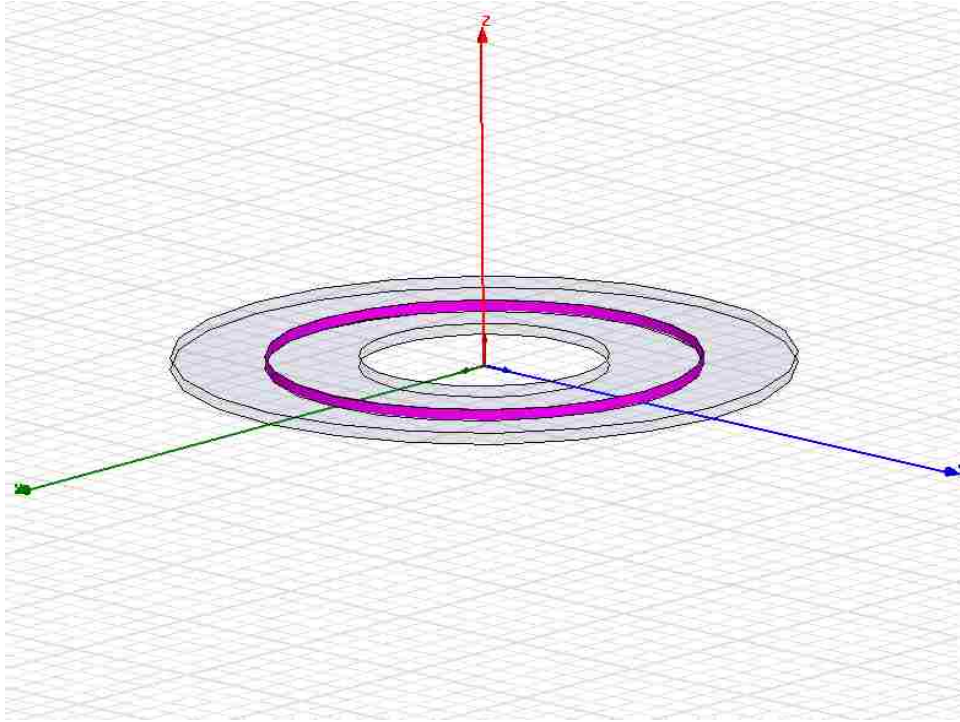


Figure 3.4 The middle radius R_{av}

There are four pairs of brushes that touch the disc. Hence, the average current that flows through each brush is:

$$I_{each} = \frac{I_a}{4} = \frac{3344}{4} = 836 \text{ A} \quad (3.4)$$

CHAPTER 4 DETERMINATION OF ELECTROMECHANICAL PARAMETERS OF THE MOTOR

4.1 Motor Model in 3D FEM MAXWELL

As the twin-rotor homopolar DC motor model is developed in 3D FEM, a condition for current flow in the aluminum discs cannot be simulated in a traditional way because there are not wires spread around the discs. There are 4 pairs of brushes distributed evenly around the disc periphery. The currents do not flow through the aluminum disc radially because the width of their paths is changing with the radius. Also, the MAXWELL software does not allow on physical contact of two different conducting materials. To solve this problem, the conducting disc with the brushes was modeled by aluminum disc with 4 pairs of rectangular boxes as shown in figure 4.1

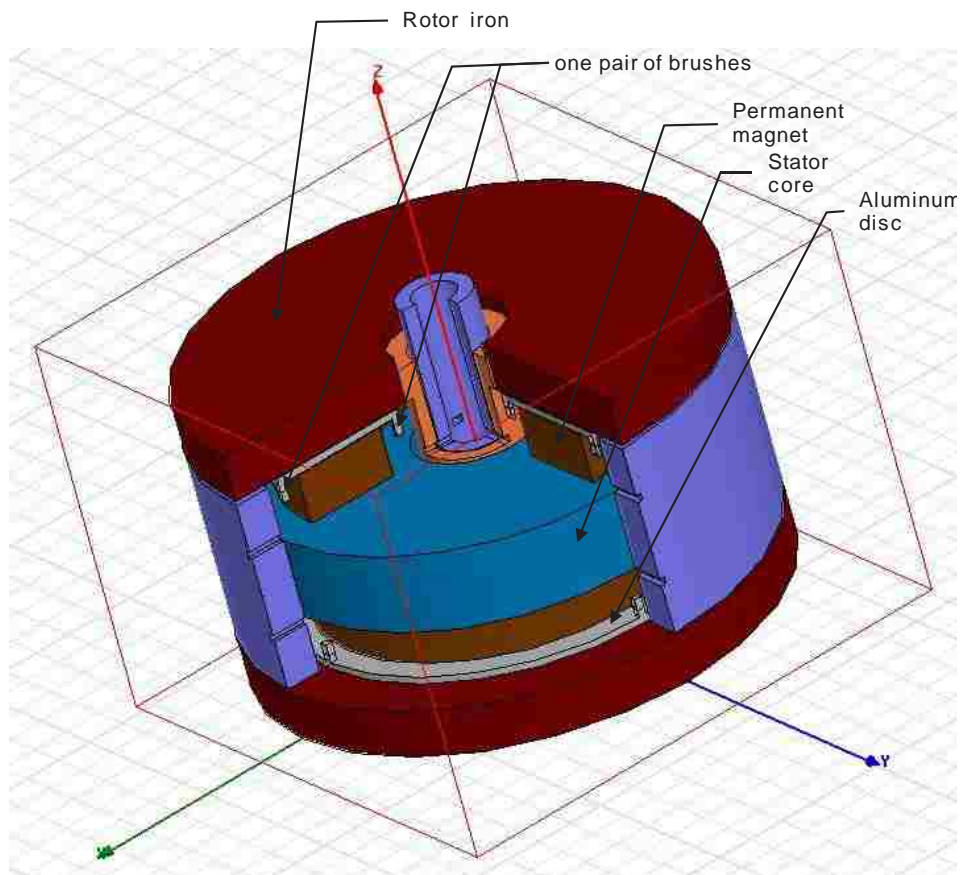


Figure 4.1 Twin-Rotor homopolar DC motor model

4.2 Currents Density Distribution in Aluminum Discs

As it was mentioned in the section on 3D FEM modeling, the current is entering each disc in four points at the disc periphery (see figure 4.2). It was assumed that the total current flowing radially through the disc was equal to 3344 A. It means that the current entering one point on the rotor disc was equal to 836 A.

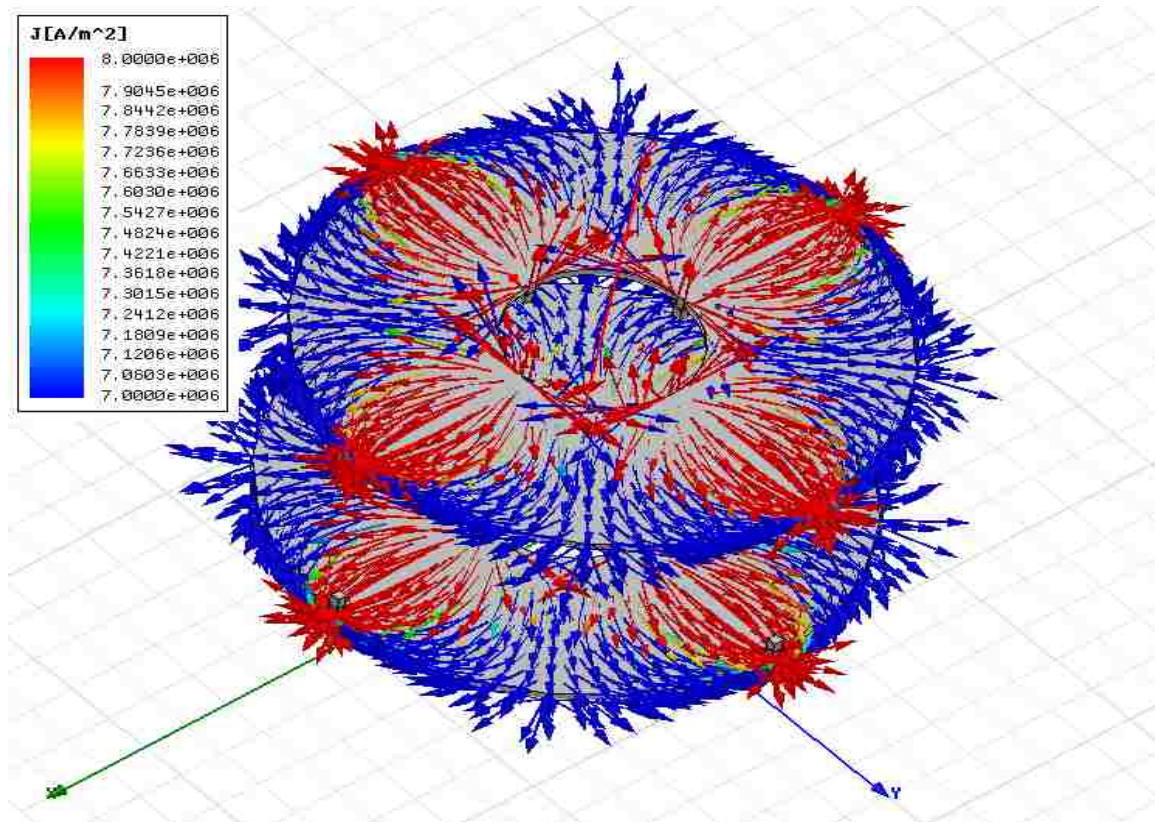


Figure 4.2 The distribution of current density in the aluminum discs

The currents flow through the disc along the arc paths giving the highest current density along the shortest path. This unevenly distributed current density may contribute uneven distribution of power losses in the discs and consequently to the local over-heating. The figure 4.3 shows the ohmic power losses distribution in the disc, which concentrate in the area of higher current density. The local over-heating may lead to the mechanical distortion of the aluminum discs and consequently to the motor failure. The non-radial distribution of

currents contributes also to non-uniform distribution of force density. This will affect the resultant force produced by the motor, which is expected less than the force in case of uniformly distributed currents that flow in the wire of conventional motors.

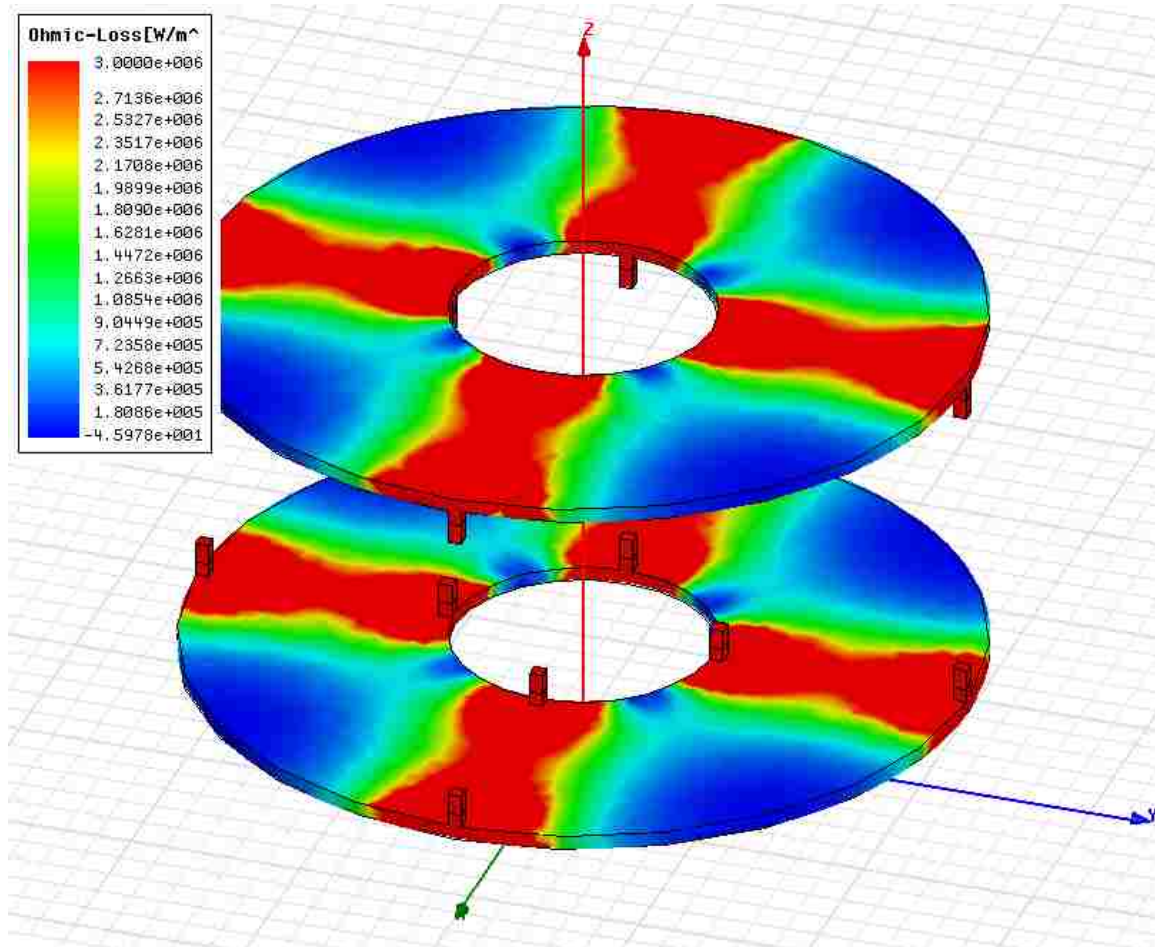


Figure 4.3 Ohmic power losses distribution in the discs

4.3 Magnetic Flux Density Distribution in the Motor

For the motor operation an important role plays the magnetic flux density distribution. The picture of the magnetic field density in the whole volume of the motor informs which part of the motor is saturated. As an example, a magnetic flux density distribution in the stator disc is shown in figure 4.4. The vectors that represent the flux density are distributed outwards on both sides of the disc because the magnets attached to the disc were magnetized axially in opposite directions. At the stator disc periphery, the flux density vectors are

directed radially because the magnetic flux is closed throughout the stator external cylinder.

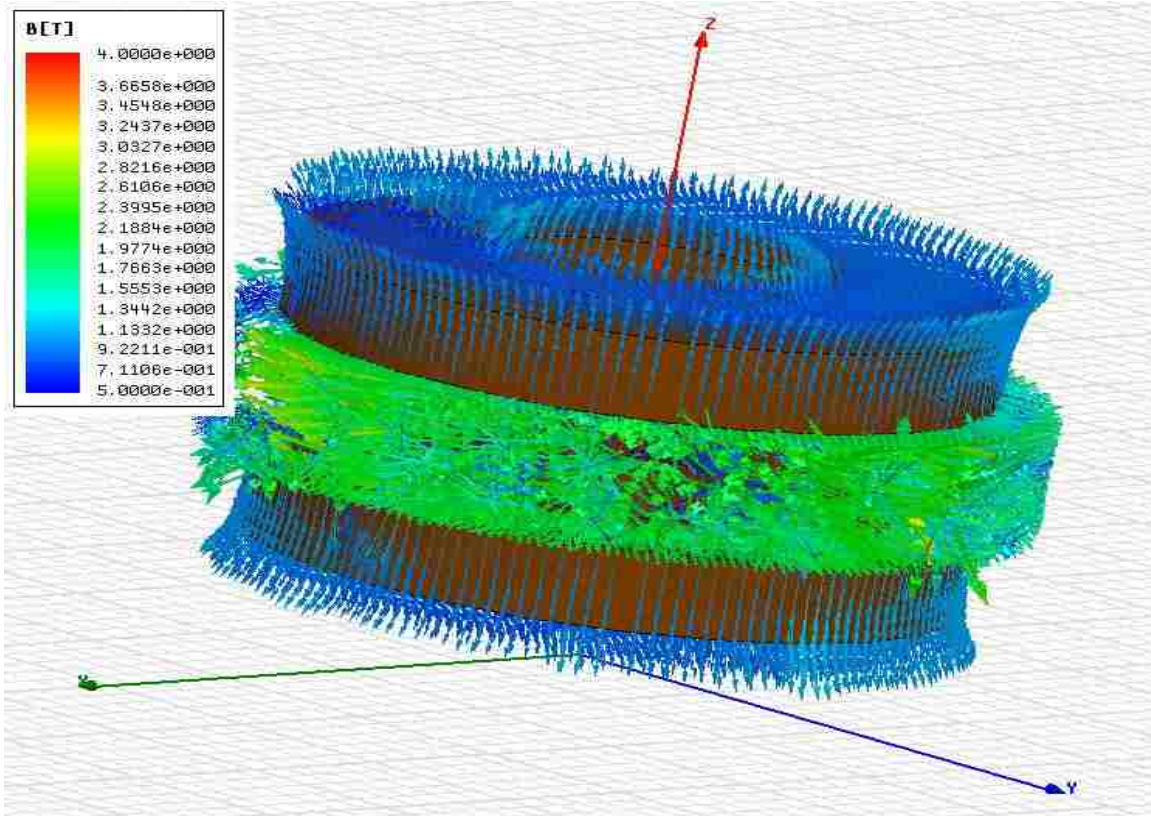


Figure 4.4 Magnetic flux density distributions in the motor

The most important information is how the magnetic flux density is distributed inside the aluminum disc. This decides about the distribution of the force density f_{em} in the disc volume, which is expressed by the equation:

$$f_{em} = J \times B \quad (4.1)$$

where: J - the current density

B – the flux density

The figure 4.5 shows the flux density distribution in the aluminum discs. This flux is perpendicular the disc surface and is distributed evenly around the disc. At the edges, it changes its direction and the average flux density on the rotor disc is 0.8 T, the value that was assumed.

4.4 Electromagnetic Forces and Torque in the Motor

4.4.1 Provisional Torque Calculation

The electromagnetic Lorentz force acting on the aluminum disc of the rotor can be determined from the basic equation:

$$F = B \cdot L \cdot I \quad (4.2)$$

where: L is the active length at the conductor carrying current I_a , which in case of conducting disc is:

$$\begin{aligned} L &= (R_{outer} - l_1) - (R_{inner} + l_2) \\ &= (0.057 - 0.001) - (0.019 + 0.001) = 0.036 \text{ m} \end{aligned} \quad (4.3)$$

$$\text{where } l_1 = \frac{\text{outside brushless length}}{2}$$

$$l_2 = \frac{\text{inner brushless length}}{2}$$

In case of aluminum disc the total current flowing radially through the disc is 3344 A. The disc width being within the influence of the magnetic field is of 0.036 m. The magnetic flux density $B = 0.8$ T as the figure 4.4 shown. Thus the electromotive force and the total torque exerting on the disc is:

$$\begin{aligned} F_{em} &= B \cdot L \cdot I_a \\ &= 0.8 \cdot 0.036 \cdot 3344 = 96.3 \text{ N} \end{aligned} \quad (4.4)$$

$$\begin{aligned} T_{em} &= F_{em} \cdot R_{av} \\ &= 96.3 \cdot 0.038 = 3.659 \text{ N} \cdot \text{m} \end{aligned} \quad (4.5)$$

4.4.2 Forces and Torque Determination using FEM

The electromagnetic torque is the product of current and magnetic flux density. In general, the magnetic flux density is evenly distributed over the entire aluminum disc (see figure 4.5), but the current is far from uniform distribution (see figure 4.2). It means that the

force density distribution will be similar as the current density distribution shown in figure 4.2. But it is directed perpendicularly to the B and J.

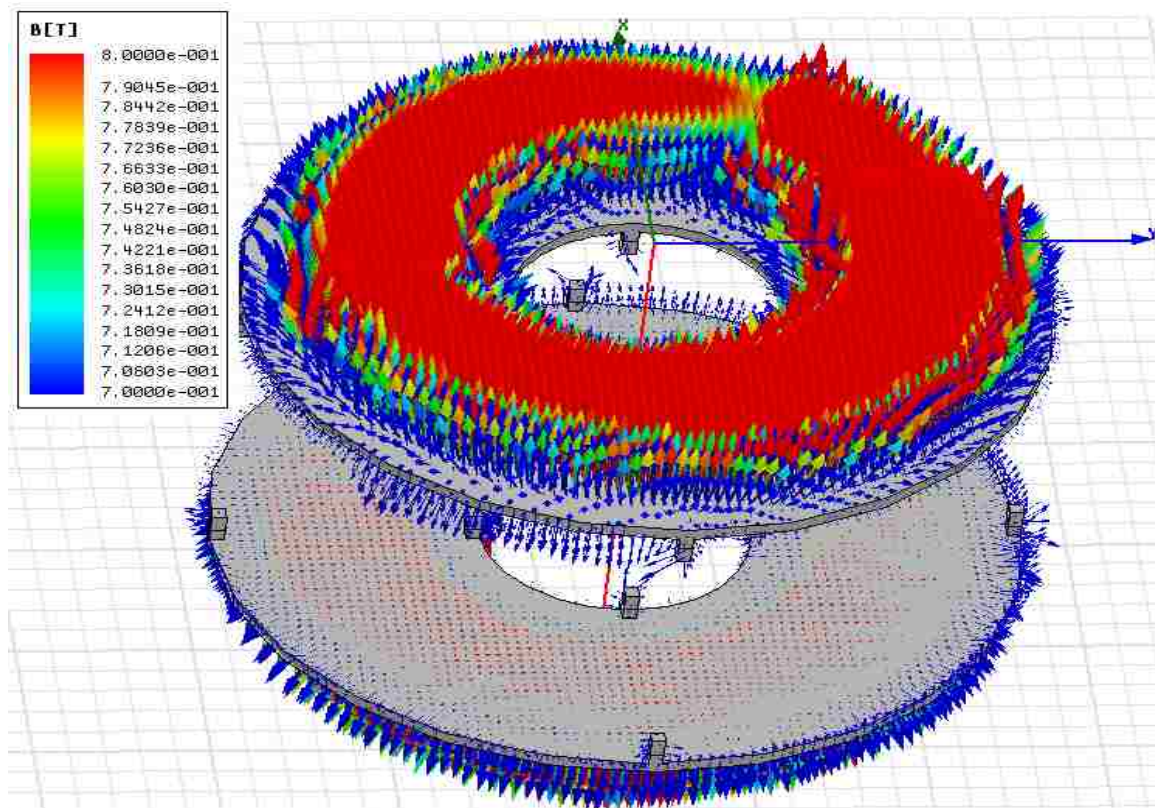


Figure 4.5 Magnetic flux distributions on the aluminum discs

The total torque acting on one disc rotor is equal to $1.851 \text{ N} \cdot \text{m}$. There is also very strong attractive force exerting on the ferromagnetic rotor disc in axial direction. It's value is 3821.6 N . The bearing of rotor disc must withstand this force, thus special type of them have to be applied.

4.4.3 Discussion on Discrepancies between Rough Assessment and FEM Results

Looking at the results of electromagnetic torque obtained from provisional assessment (section 4.4.1) and from calculations using Maxwell 12v software a significant discrepancy is seen. One of the reasons can be the accuracy of torque calculation used in both methods. Another reason is just a non uniform distribution of radial current component over the entire

aluminum disc.

One more and perhaps most vital reason is the current paths, which are mostly far from being radially directed as it was assumed in provisional calculations. As it was shown in figure 4.6, the current flows in radial direction only through the narrow path between + and – polarity brushes. Mostly the current flows along the paths as shown in figure 4.7. The electromagnetic force is directed perpendicularly to the current path. Due to the curvature of this path, the force can be split into two components: one, tangential to be radius (F_T) and another, radially directed (F_r). Only tangential component contributes to the torque according to equation

$$T_{em} = \int_{R_{in}}^{R_{out}} r \cdot dF \cdot \cos\beta(r) \quad (4.6)$$

where:

$$dF = B \cdot i \cdot dr \quad (4.7)$$

r – radius at which the increment force dF is calculated.

β – angle (see figure 4.7) which is the function of radius.

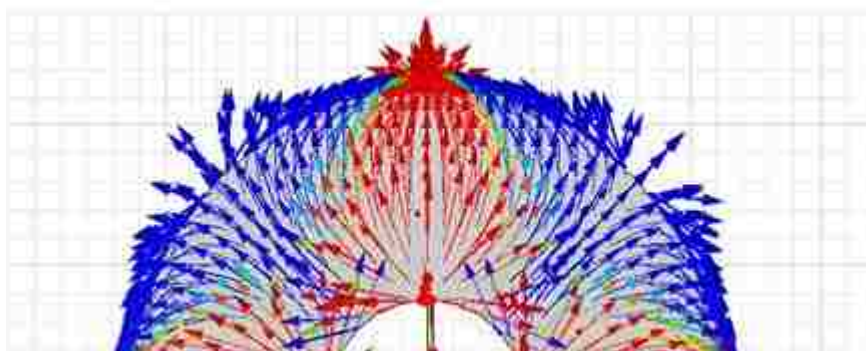


Figure 4.6 One specified part of the current flux density distribution

The total radial component F_r is zero since its value above average radius R_{av} is positive and below R_{av} is negative.

Summarizing, the total torque calculated using Maxwell 12v has to be smaller than the

torque assessed under assumption that the current is flowing through the rotor disc in radial direction only.

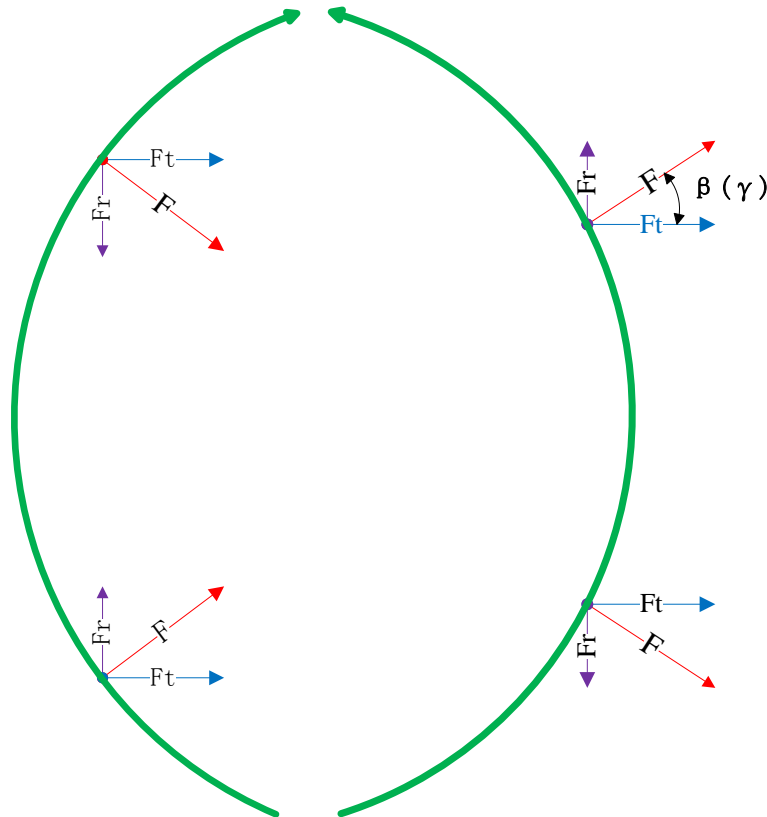


Figure 4.7 Left-hand and right-hand symmetrical current flow paths

4.5 Determination of the Motor Equivalent Circuit Parameters

- **Armature Resistance**

The disc resistance depends on how the current flows. Since it flows radially, the cross-section area of the disc in this direction is varying with disc radius. Thus, the resistance that varies with the radius can be expressed by the following equation:

$$R_{disc} = \int_{r_1}^{r_2} \frac{dr}{\gamma \cdot A(r)} \quad (4.8)$$

since

$$A(r) = 2\pi r \cdot d \quad (4.9)$$

The disc resistance is:

$$R_{disc} = \int_{r_1}^{r_2} \frac{1}{\gamma \cdot 2\pi r \cdot d} dr = \frac{\ln|r|}{\gamma \cdot 2\pi \cdot d} \Big|_{r_1}^{r_2} = \frac{1}{\gamma \cdot 2\pi \cdot d} (\ln r_2 - \ln r_1) \quad (4.10)$$

where $d = 2 \text{ mm}$, disc thickness.

$\gamma = 3.8 \times 10^7 \text{ Siemens/m}$, electrical conductivity of the disc

$r_1 = 19 \text{ mm}$; $r_2 = 57 \text{ mm}$; (See figure 4.8)

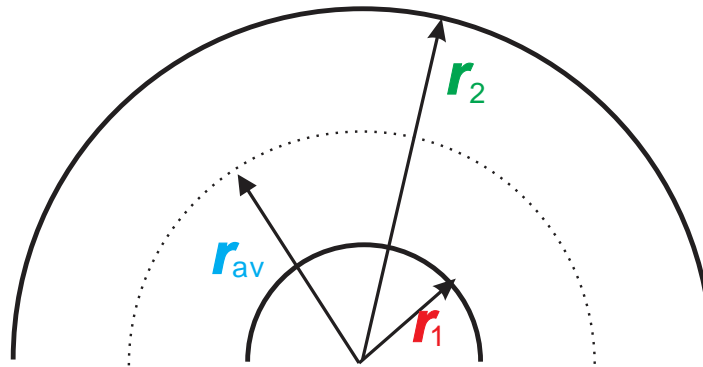


Figure 4.8 Explanation of equation (4.10)

Substituting the numbers to equation 4.10, the resistance $R_{disc} = 2.30 \cdot 10^{-6} \Omega$

The resistance can be assessed also using the simplified approach, namely:

$$R_{disc} = \frac{(r_2 - r_1)}{\gamma \cdot 2\pi r_{av} \cdot d} \quad (4.11)$$

For the average radius (see figure 4.8) $R_{av} = 38 \text{ mm}$. Hence, the resistance $R_{disc} = 2.09 \times 10^{-6} \Omega$.

The total resistance R_a is the sum of disc resistance and resistance of brushes. The last one is omitted here.

- **Armature Inductance**

Since the armature winding is in form of the aluminum disc and the inductance is proportional to the length of current path it should be very low and could be omitted in the motor equivalent circuit. Because the resistance R_a is also very low, the inductance should be taken into account. Similar as for disc resistance, the curvature of currents' path should be

included in calculation. This can be done using FEM Maxwell 12v. However, this program cannot calculate it when disc structure is considered to solve this problem. The disc was divided into 18 pieces as shown in figure 4.9.

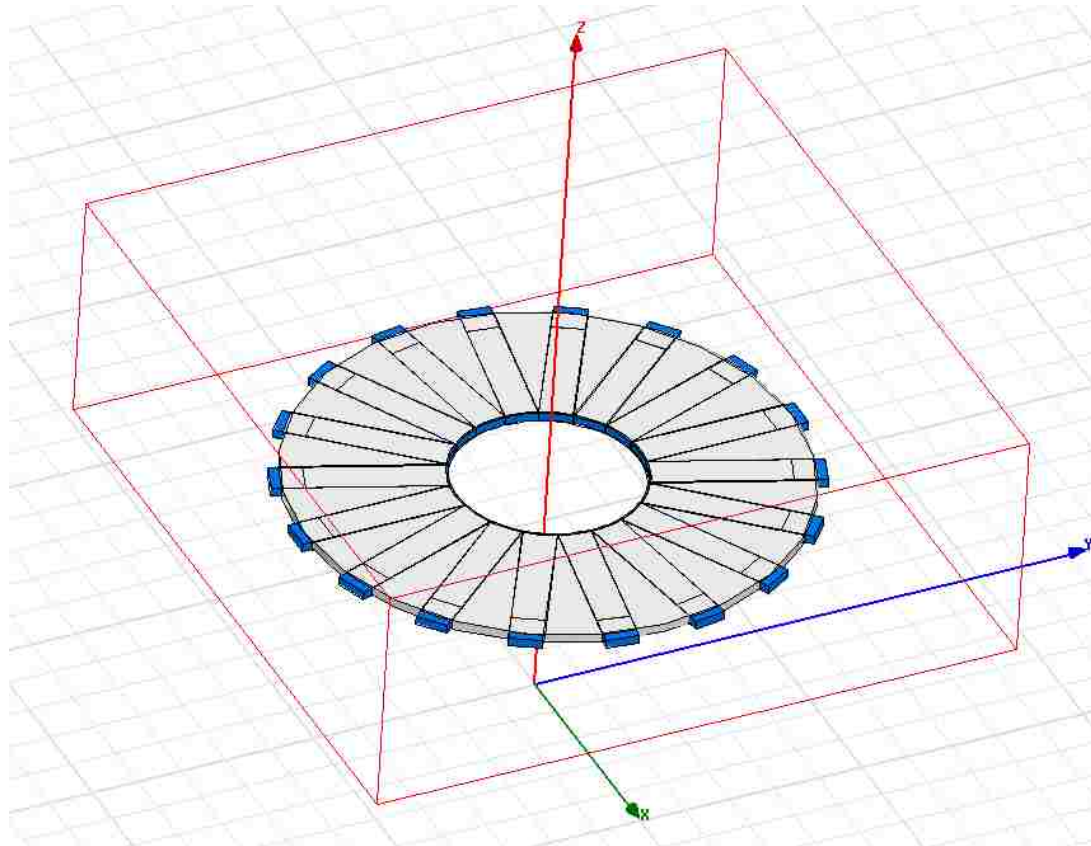


Figure 4.9 Aluminum disc shown in form of aluminum bars

From the simulation, the inductance of separate bar was obtained and was equal to $H_b = 5.249 \times 10^{-5} H$. The total inductance is the reciprocal of the sum of $1/H_b$ and is equal to $2.916 \times 10^{-6} H$.

The above mentioned approach is a simplified method, which does not take into account the curvature of current paths. The inductance L can be determined also using 2-D FEM software FEMM applying the same assumption that current paths are paralleled. The FEM model for calculating inductance is shown in figure 4.10.

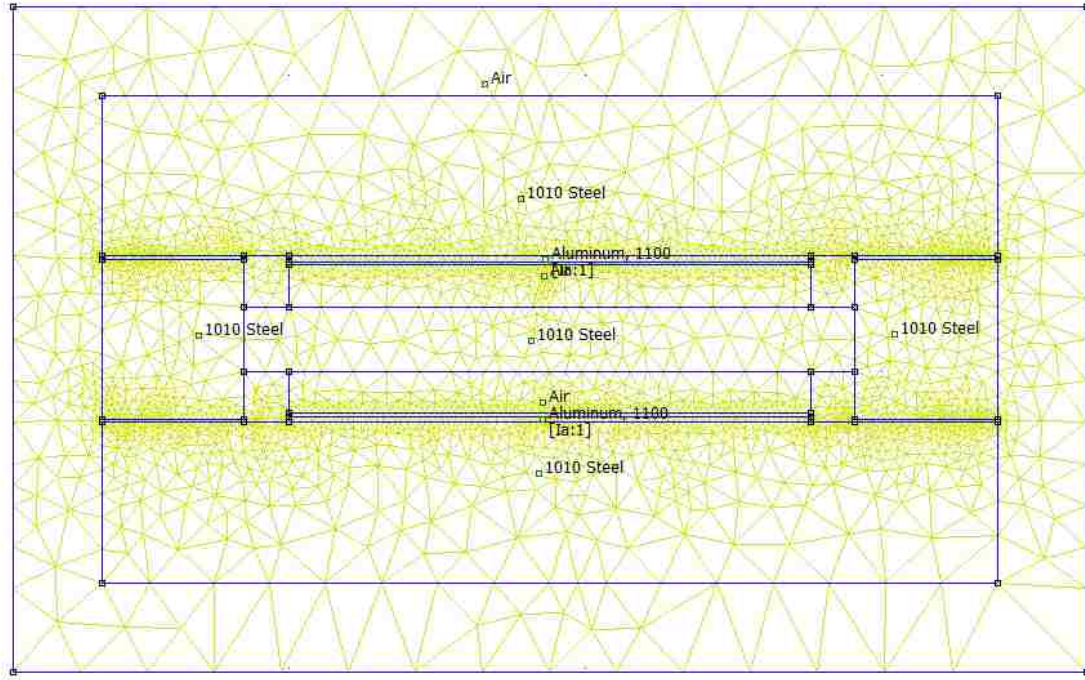


Figure 4.10 FEM model for inductance determination

The motor disc structure has been unfolded with respect to the average disc radius R_{av} and the depth of the model is equal to the aluminum ring width calculated as $r_2 - r_1$ (see figure 4.8). The permanent magnet was converted into the block with parameters of air and the rated current was assigned to the disc. The inductance obtained from simulation is $L_a = 1.32 \times 10^{-6} H$, what is different to the one obtained from MAXWELL model (figure 4.10). Because the model in figure 4.9 did not count the inductance between the aluminum separate bars, the inductance value calculated of the FEM model in figure 4.10 is more accurate.

- **Electromotive Force E_a**

The electromotive force (emf) induced in rotor disc depends on flux density distribution and the rotor speed. Since the flux density is evenly distributed in the air-gap over the area of PM, its direction is perpendicular to direction of rotor motion. In the case considered here, it is radially directed and can be calculated as:

$$E_a = \int_{r_1}^{r_2} B \cdot r \cdot \omega dr = B \cdot \omega \cdot \frac{1}{2} r^2 \Big|_{r_1}^{r_2} = B \cdot \omega \cdot \frac{1}{2} \cdot (r_2^2 - r_1^2) \quad (4.14)$$

where: $r_1 = 19 \text{ mm}$; $r_2 = 57 \text{ mm}$; (see figure 4.8)

For the motor considered here, where $B = 0.8 \text{ T}$ and $\omega_m = 200 \text{ rad/s}$, the emf

$E_a = 0.231 \text{ V}$. The emf coefficient

$$K_E = \frac{E_a}{\omega_m} = 0.001155 \text{ V/rad/s} \quad (4.15)$$

This coefficient is later used in block diagram that allows modeling the motor in dynamic conditions.

4.6 Parameters of Equivalent Mechanical System

- **Electromagnetic Torque Coefficient K_T**

The electromagnetic torque developed by the motor is proportional to the current I_a :

$$T_{em} = K_T \cdot I_a \quad (4.16)$$

For the torque of $1.851 \text{ N} \cdot \text{m}$ determined in section 4.4 at armature current $I_a = 3344 \text{ A}$, the torque coefficient is $K_T = 5.535 \times 10^{-4}$.

- **Moment of Inertia J_r**

The moment of inertia J_r of the rotor is equal to combined moment of inertia of two aluminum disc and iron disc that is calculated as follow:

The mass of a cylindrical structure of outer radius r_1 , inner radius r_2 , and thickness h depends on mass density and the volume of it. The materials density ρ [8] and the dimensions of aluminum discs and iron discs are enclosed in Table 4.1.

Hence, the moment of inertia of one rotor is:

$$J_r = \left[\frac{1}{2} m_{AL} (r_1^2 + r_2^2) + \frac{1}{2} m_{Fe} (r_3^2 + r_4^2) \right] = 0.00395 \text{ Kg} \cdot \text{m}^2 \quad (4.17)$$

where m_{Fe} and m_{AL} are mass of iron disc and aluminum disc respectively and they are calculated as follows:

$$m = \rho \cdot \pi \cdot (r_1^2 - r_2^2) \cdot h \quad (4.18)$$

where h is thickness.

Table 4.1 Aluminum discs and iron discs

	Aluminum discs	Iron disc (steel 1008)
Mass density	$\rho_{AL} = 2699 \text{ Kg/m}^3$	$\rho_{Fe} = 7872 \text{ Kg/m}^3$
Outer radius	$r_1 = 57 \text{ mm}$	$r_3 = 70 \text{ mm}$
Inner radius	$r_2 = 19 \text{ mm}$	$r_4 = 14 \text{ mm}$
Thickness	$h_{AL} = 2 \text{ mm}$	$h_{Fe} = 13 \text{ mm}$

- **Friction Coefficient B**

The friction of the rotor experiences comes from bearings and the friction between rotating disc and air. This can be determined only for the real, physical object. For simulation purposes, it was assumed that the friction consists of discous friction only and is proportional to speed according to equation

$$T_{friction} = B \cdot \omega_m \quad (4.18)$$

The friction coefficient is assumed to be $B = 0.002 \text{ T/rad/s}$

To summarize, the parameters of electric equivalent circuit and mechanical system are shown in Table 4.2

Table 4.2 Parameters of electric equivalent circuit and mechanical system

Electric circuit parameters:	
- Armature resistance R_a	$2.30 \cdot 10^{-6} \Omega$
- Armature inductance L_a	$1.32 \cdot 10^{-6} H$
- Emf coefficient K_E	$0.001155 V/rad/s$
Mechanical system parameters	
- Electromagnetic torque coefficient K_T	$5.535 \cdot 10^{-4} Nm/A$
- Rotor moment of inertia J_r	$0.00395 Kg \cdot m^2$
- Friction coefficient B	$0.002 N \cdot m/rad/s$

CHAPTER 5 MOTOR PERFORMANCE IN STEADY-STATE AND DYNAMIC CONDITIONS

In the previous chapter, the magnetic field theory was used to determine the parameters of electric circuit and mechanical system. In this chapter, the analysis of motor in steady-state and in dynamics conditions will be done for motor with single rotor only using the circuit theory. This approach requires to apply the circuit model of the motor. The Maxwell 12v software of Ansoft company helped to find the parameters of the equivalent circuit. Although Ansoft company provides Simplorer software for dynamic simulation, MATLAB SIMULINK is used to simulate the motor operation in steady-state and dynamic conditions.

5.1 Motor Performance in Steady-State Condition

The operation of the PM homopolar DC motor in steady-state conditions can be analyzed using the equivalent circuit of the armature equivalent circuit of the armature winding shown in figure 5.10

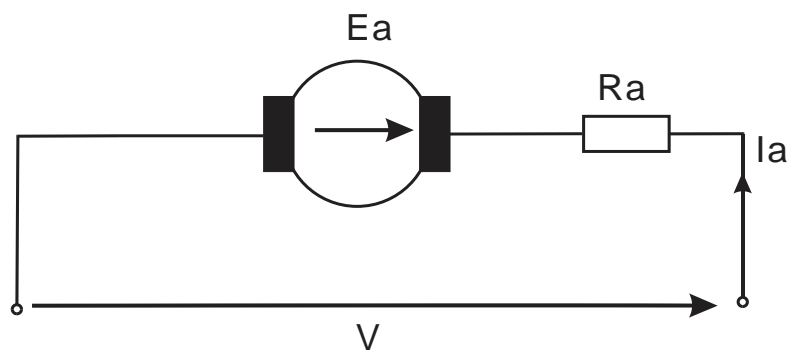


Figure 5.1 The motor equivalent circuit in steady-state

The voltage equation for the armature circuit is

$$V = E_a + R_a i_a \quad (5.1)$$

The resistance R_a also includes the resistance of contact between brushes and rotating disc which should be much lower than resistance of armature disc.

From equation 4.15, knowing that $E_a = K_E \cdot \omega_m$, a speed can be determined:

$$\omega_m = \frac{V - R_a I_a}{K_E} \quad (5.2)$$

The torque T_{out} on the rotor shaft equals to electromagnetic torque T_{em} deminished by friction torque according to equation:

$$T_{out} = T_{em} - B\omega_m \quad (5.3)$$

Since $T_{em} = K_T I_a$, the torque on the shaft is:

$$T_{out} = K_T I_a - B\omega_m \quad (5.4)$$

The output power

$$P_{out} = T_{out} \cdot \omega_m \quad (5.5)$$

The input power is given by equation:

$$P_{in} = V \cdot I_a \quad (5.6)$$

The motor efficiency is calculated from equation:

$$\eta_{\%} = \frac{P_{out}}{P_{in}} \cdot 100\% \quad (5.7)$$

The equations above allow analyzing the motor behavior in steady-state conditions. The characteristics that illustrate it are shown in figure 5.2 and 5.3 respectively. These are as follows:

$\omega_m = f(T_{out})$ rotary speed vs. output torque characteristic;

$I_a = f(T_{out})$ armature current vs. output torque characteristic;

$P_{out} = f(T_{out})$ output power vs. output torque characteristic;

$P_{in} = f(T_{out})$ input power vs. output torque characteristic;

$Eff = f(T_{out})$ efficiency vs. output torque characteristic.

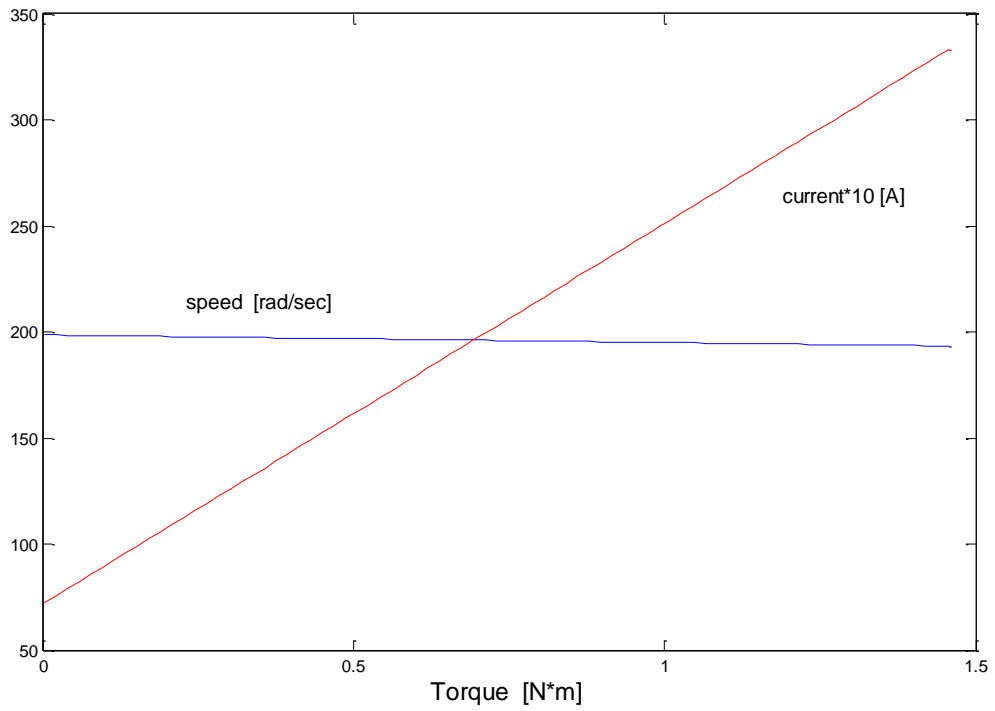


Figure 5.2 Characteristics of angular speed and armature current vs. load torque on shaft

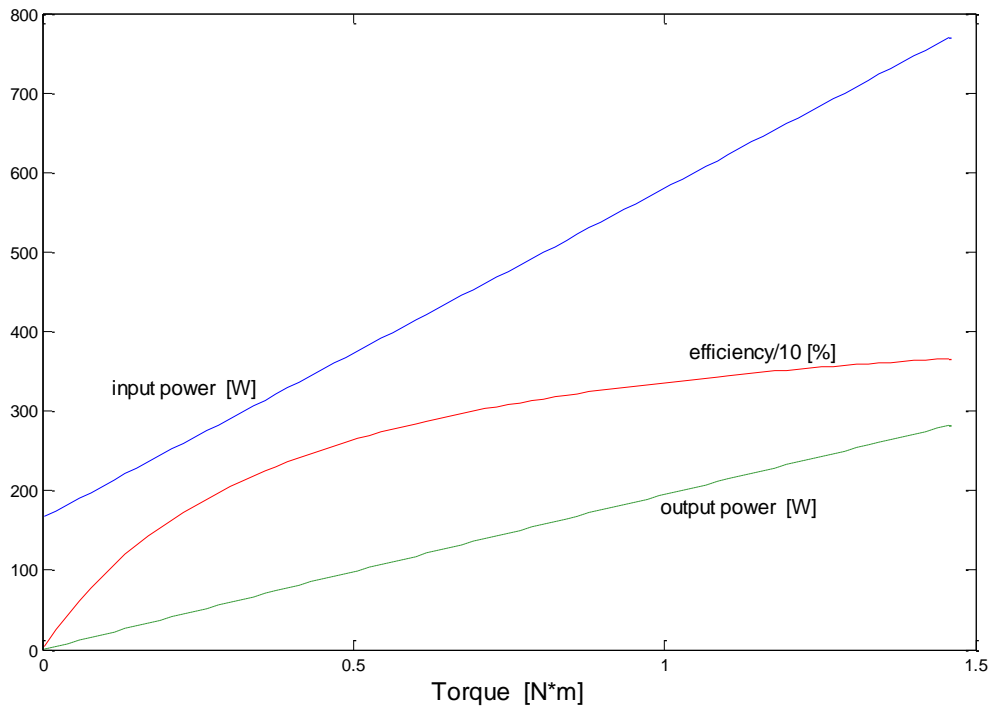


Figure 5.3 Characteristics of input power, out power and efficiency vs. load torque on shaft

These characteristics were determined using MATLAB. The code that was written is enclosed in Appendix A. The electromechanical parameters at rated conditions are enclosed in Table 5.1.

Table 5.1 Electromechanical parameters

Supply Voltage (V)	Armature Current (A)	Output Power (W)	Rotary Speed (rpm)	Motor Efficiency (%)
0.231	3344	281.76	1910	36.61

5.2 Analysis of Motor Performance in Dynamic Conditions

The equivalent circuit of the motor for dynamic analysis is shown in figure 5.4

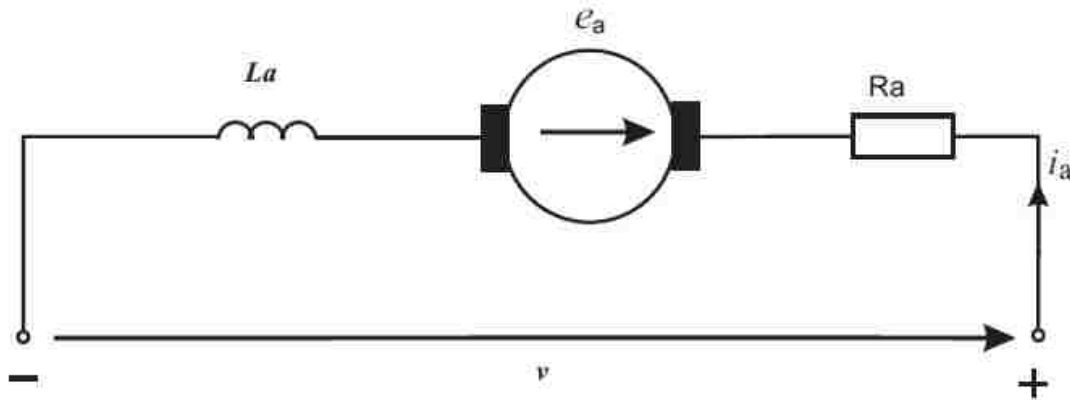


Figure 5.4 Equivalent circuit of homopolar DC motor for dynamic analysis

The equations that define the motor circuit model are as follows

$$v = e_a + R_a i_a + \frac{di_a}{dt} L_a \quad (5.8)$$

The voltage equation written in Laplace domain:

$$i_a(s) = \frac{v(s) - e_a(s)}{R_a + sL_a} \quad (5.9)$$

where $e_a = K_E \cdot \omega_m$.

The figure 5.5 shows the mechanical system of the motor with the load.

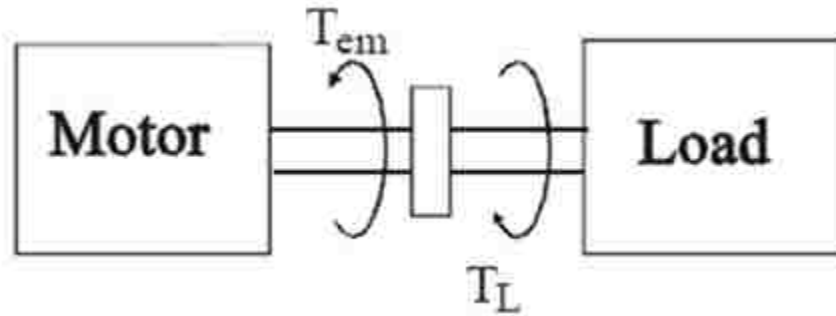


Figure 5.5 Mechanical equivalent system of homopolar motor

The equilibrium equation for the mechanical system is as follows:

$$T_{em} = T_L + J_r \frac{d\omega_m}{dt} + B\omega_m \quad (5.10)$$

Torque equations written in Laplace domain has the form:

$$T_{em}(s) - T_L(s) = sJ_r\omega_m(s) + B\omega_m(s) \quad (5.11)$$

The rotor speed is:

$$\omega_m = \frac{T_{em} - T_L}{sJ_r + B} \quad (5.12)$$

Where: J_r is moment of inertia of the motor.

B is combined friction coefficient of the rotary motion system.

T_{em} is electromagnetic torque developed by the motor. It is expressed by the equation

$$T_{em} = K_T \cdot i_a.$$

T_L is a load torque

With respect to the above equations the block diagram of homopolar DC motor was developed as shown in figure 5.6.

To simulate the motor dynamics, the block diagram in SIMULINK was developed. It is shown in figure 5.7.

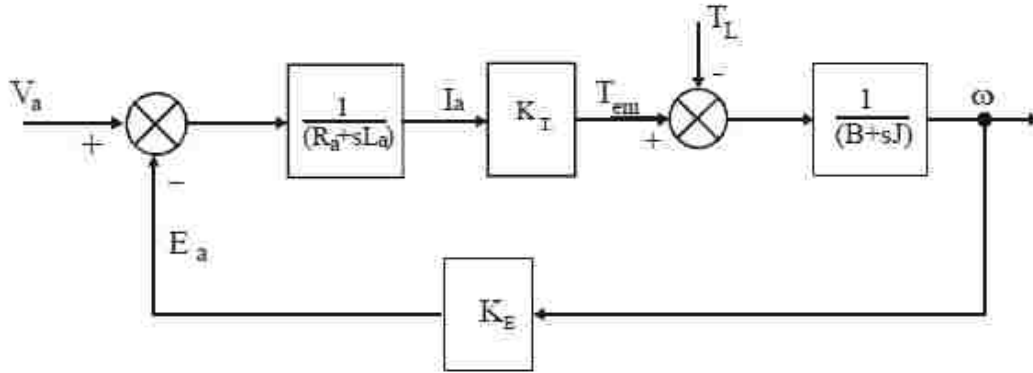


Figure 5.6 Block diagram of homopolar DC motor

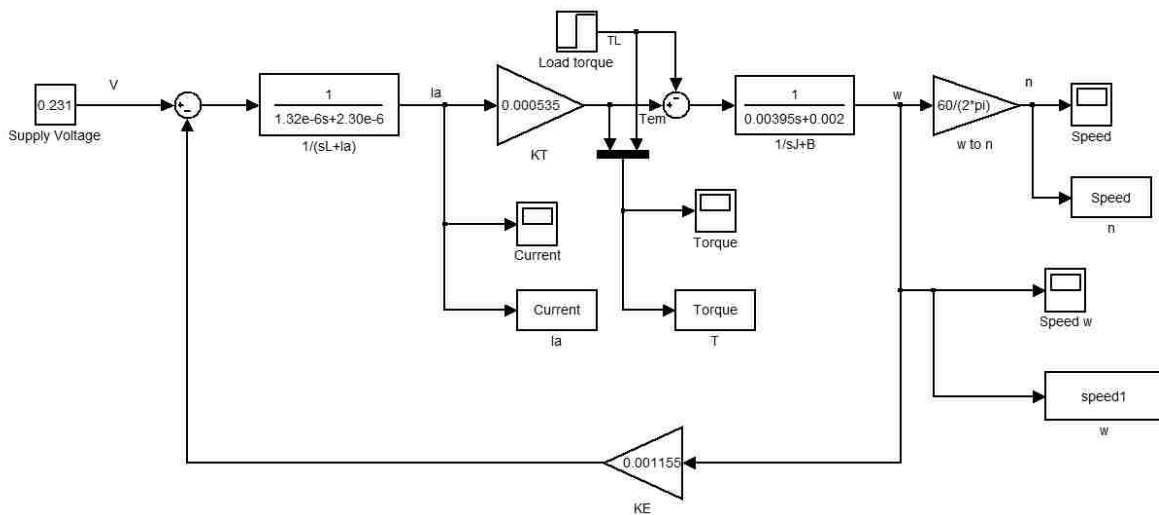


Figure 5.7 Simulink block diagram of homopolar DC motor for analysis in dynamic condition

Initial setup for the dynamic model: the homopolar DC motor is starting with no-load being supply by voltage of 0.231 V, and after the system reaches a steady-state, the load of $1.4 \text{ N} \cdot \text{m}$ is attached to the rotors. The results of simulation are shown in figure 5.8 and 5.9 in form of rotary speed, electromagnetic torque and armature current. It can be seen that when the motor is starting it has an initial torque of $7.669 \text{ N} \cdot \text{m}$ because the starting current is high equal to $1.433 \times 10^4 \text{ A}$. After 6 second, the motor reaches the steady-state. At 10 seconds, the load torque of $1.4 \text{ N} \cdot \text{m}$ is applied and the speed decreases to the rated speed, while the electromagnetic torque and current are rising to the rated values.

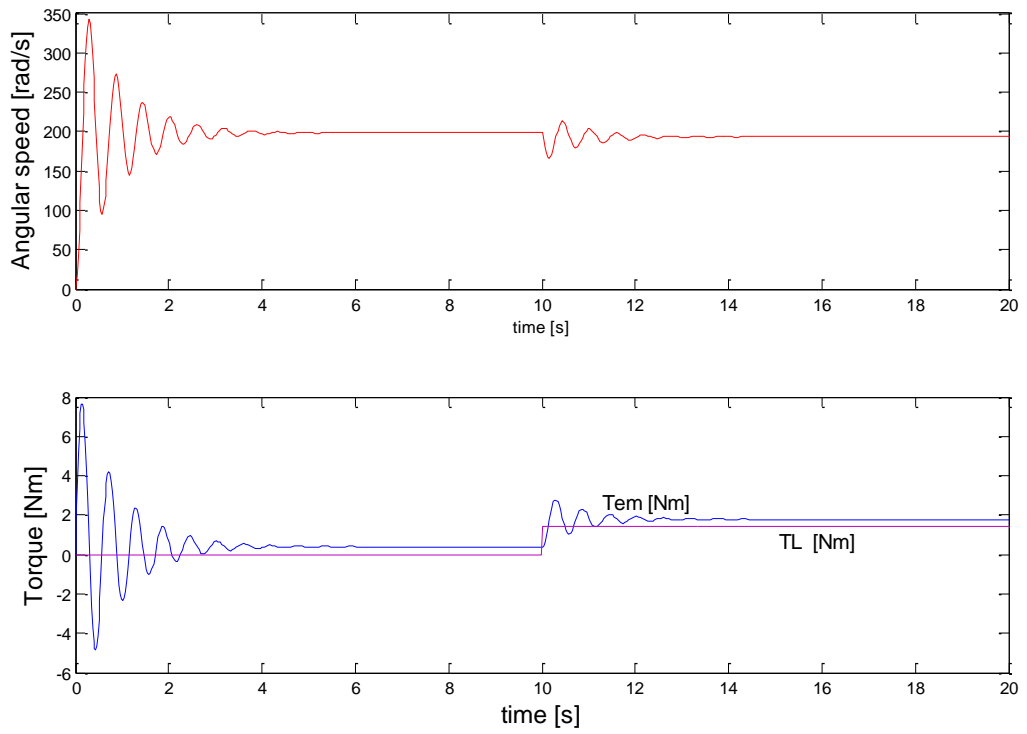


Figure 5.8 Angular speed, electromagnetic torque and load torque waveforms

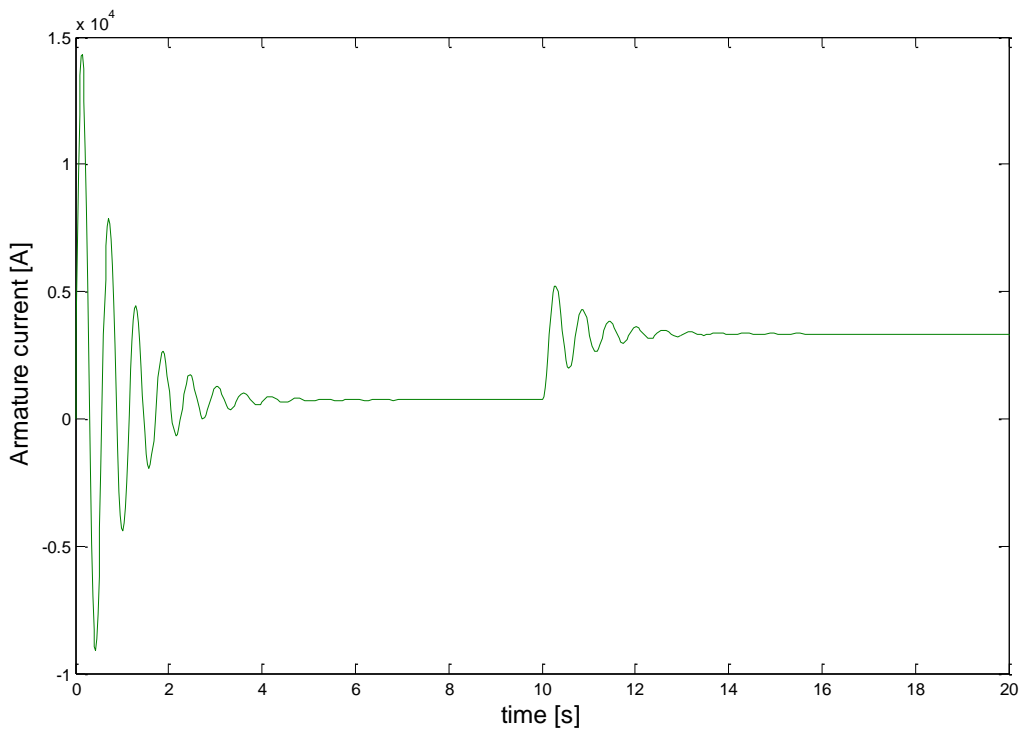


Figure 5.9 Armature current vs. time characteristics

At starting the current in the aluminum disc much exceeds the rated steady-state value.

This may overheat the aluminum disc and damage the rotor disc mechanically due to high starting torque. To avoid this, a gradually increase of supply voltage is applied. Figure 5.10 shows the ramped start-up process simulated using block diagram presented in figure 5.11. This time the current does not exceed 868 A at starting.

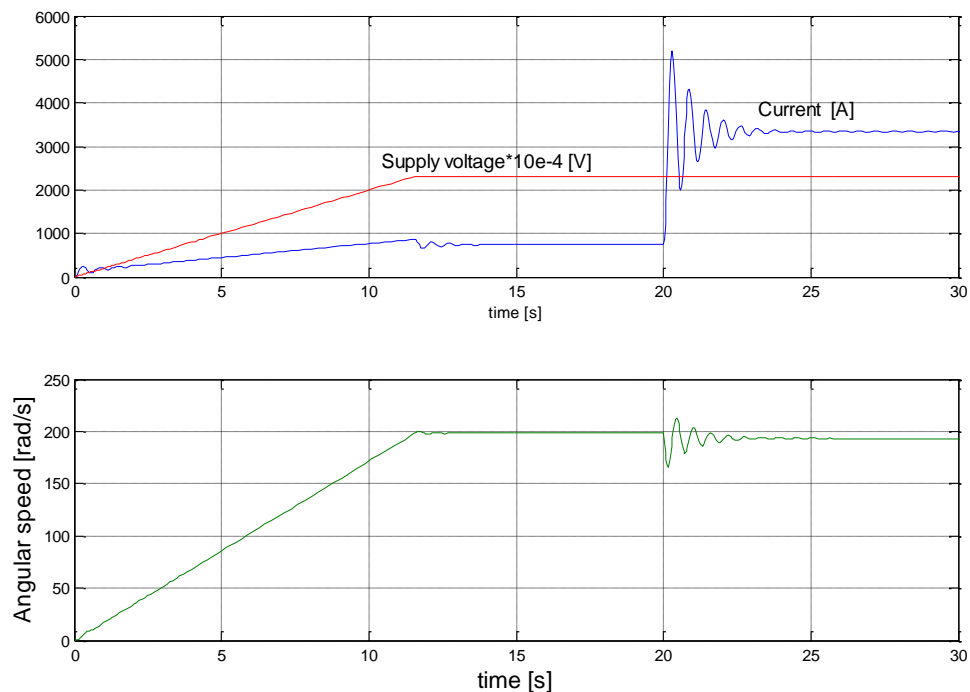


Figure 5.10 Current, supply voltage and speed characteristic with ramped start-up

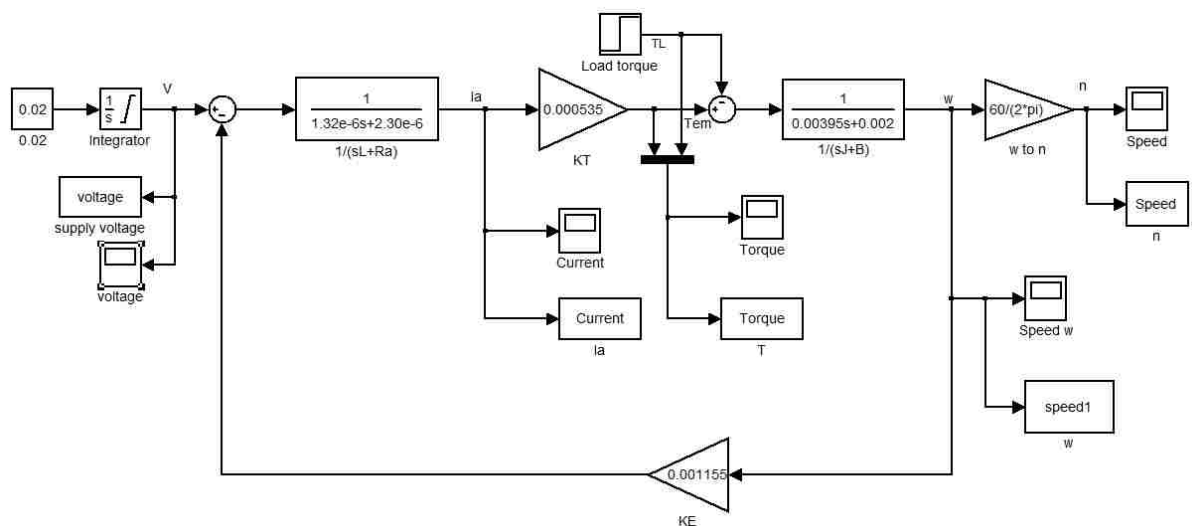


Figure 5.11 Block diagram for ramped start-up

5.3 Verification of Simulation Results

To rely on results obtained from simulation, a physical model of the motor has to be built and relevant measurement should be carried out. So far this type of model has not been built.

However, a model of slightly modified construction is available (see figure 5.12).

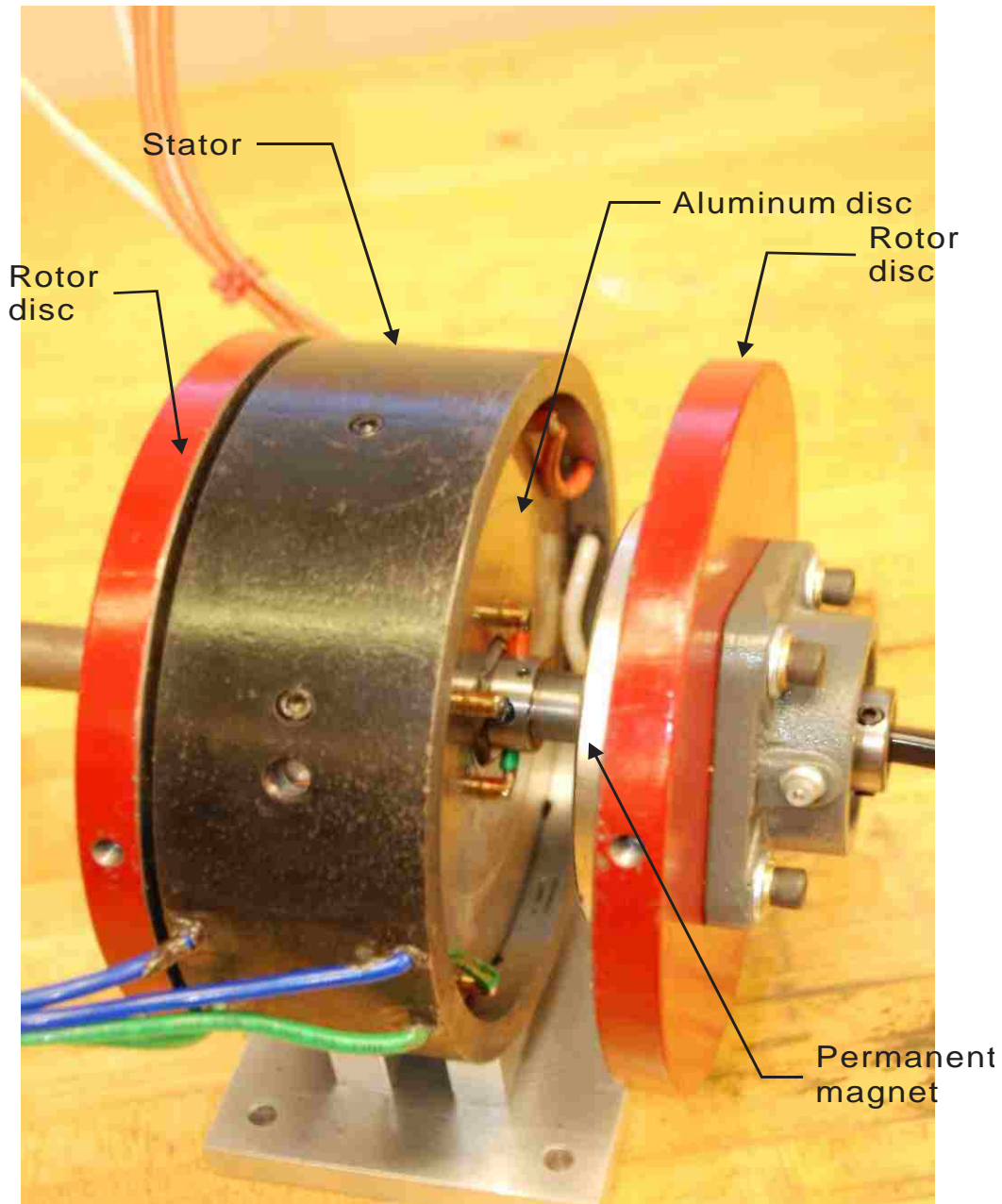


Figure 5.12 The real model of twin-rotor homopolar DC motor in LSU Power Lab

This model differs from the one analyzed in this thesis by the elements of stator and rotor. The aluminum discs in this model are attached to stator iron core while the permanent

magnets are glued to the rotor iron discs as it is shown in motor scheme presented in figure 5.13.

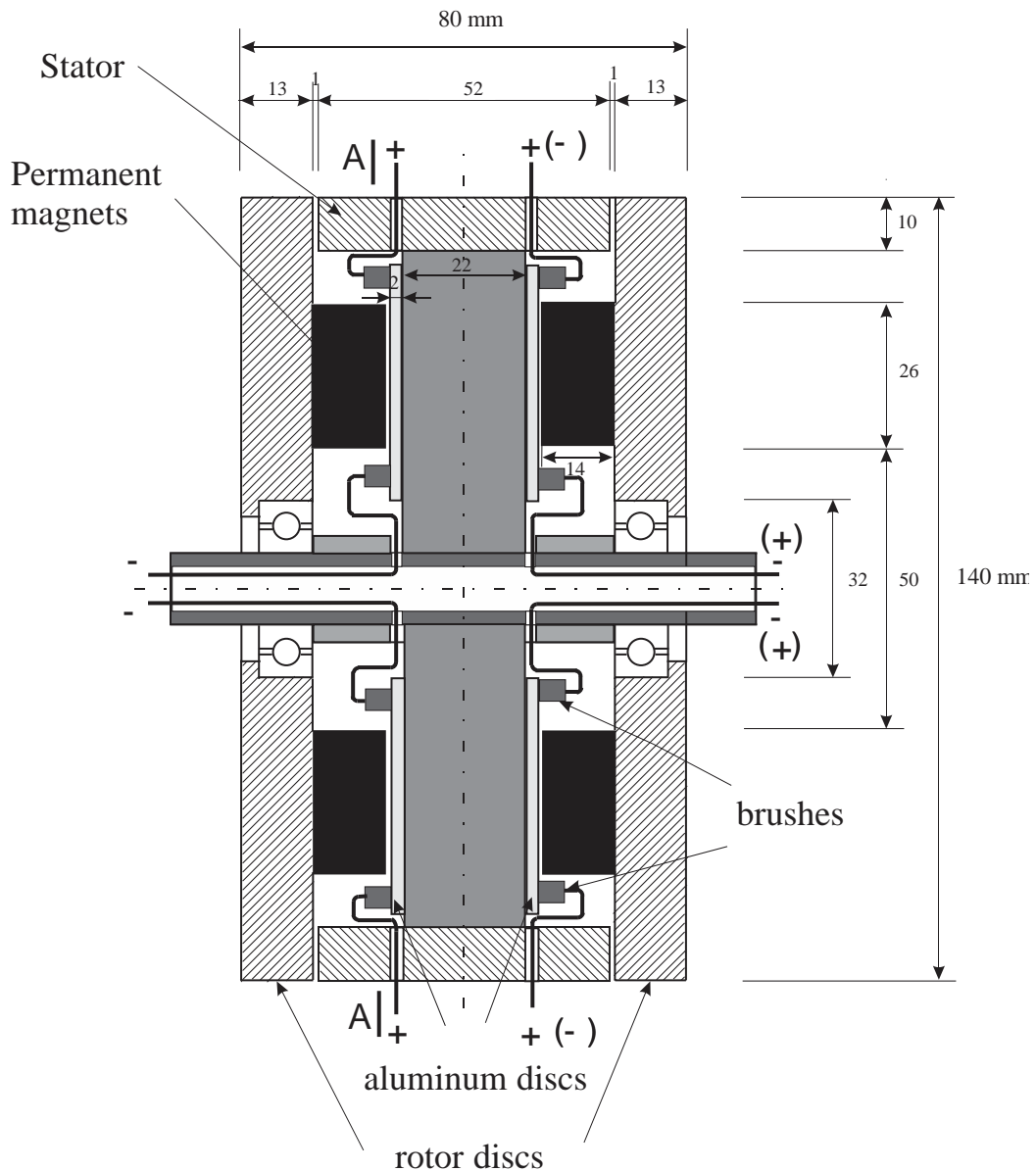


Figure 5.13 Scheme of the PM homopolar motor with the aluminum disc mounted to the stator (M-point of measurement)

All dimensions of motor elements are the same for the motor which discussed here. Thus, some of quantifies are the same in both versions. One of these is the magnetic flux in gap between stator core and rotor core (see figure 5.13 point M). The magnetic flux density distribution in radial direction determined applying FEM software femm is shown in figure

5.14. The femm model of the motor is shown in figure 5.15.

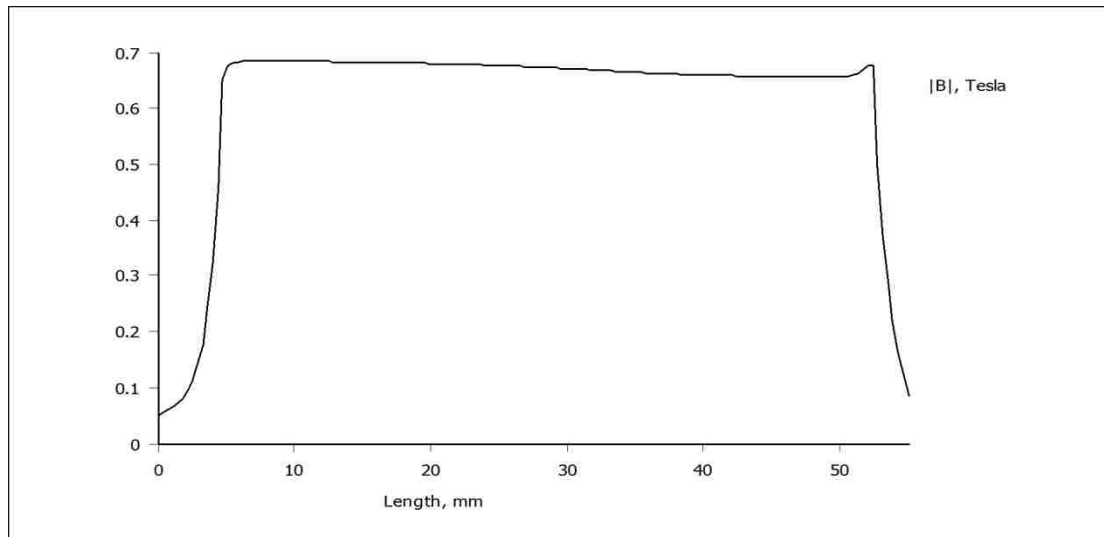


Figure 5.14 flux density distribution in radial direction in femm software

The measured flux density in this point is $B = 0.78 T$, very close to that determined from simulation. This validates to some extent the simulation model used to analyze motor electromechanical parameters.

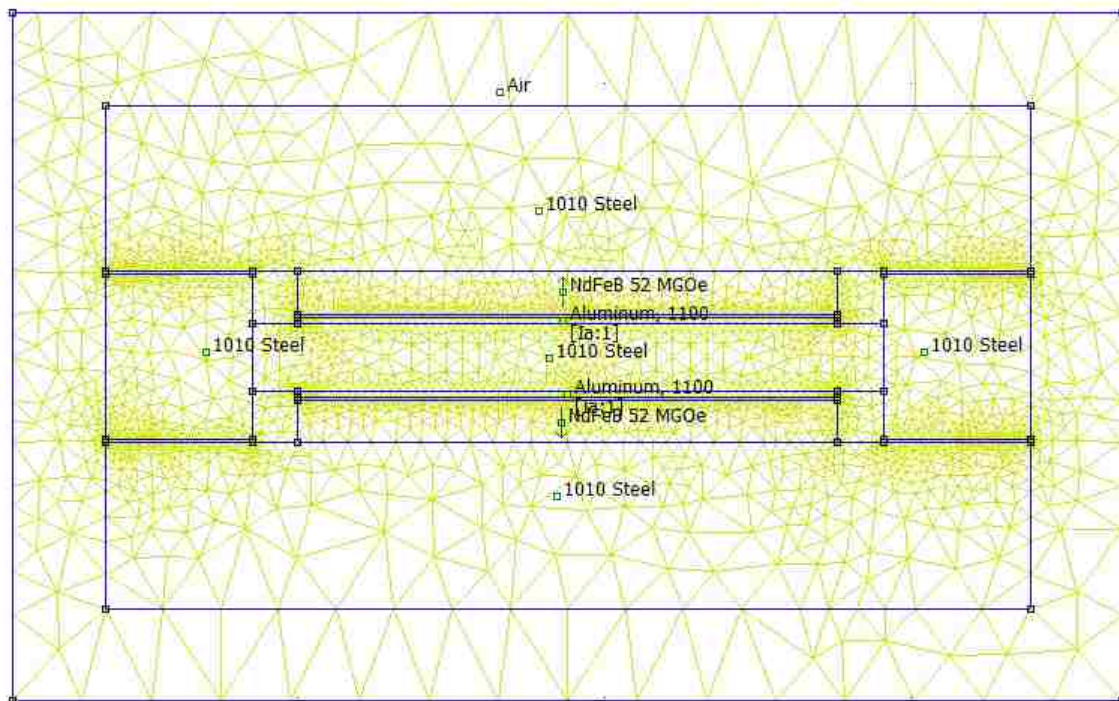


Figure 5.15 Femm software model of the motor with aluminum discs on the stator

CHAPTER 6 CONCLUSIONS AND FUTURE WORK

6.1 Conclusions of the Twin-Rotor Homopolar DC Motor

The performance of PM twin-rotor homopolar disc DC motor has been studied in this thesis. The field theory and circuit theory was applied to determine the motor electromechanical characteristics. The field theory was used to determine mainly the parameters of the equivalent circuit and 3D FEM was applied to solve the Maxwell's differential equations. The circuit model was used to analyze the motor performance in dynamic and steady-state conditions.

Form the analysis the following conclusions can be deduced:

- To produce the electromagnetic torque, the rotor aluminum discs have to be supplied by very high currents. This is the major deficiency of this motor. The advantage is, that there is no commutator, which must be applied in conventional DC machines.
- The current is not uniformly distributed in the rotor disc what leads to the smaller torque developed by the motor. To improve this, more brushes should be applied around the aluminum disc periphery.
- Nonuniform distribution of current also leads to nonuniform power loss distribution in aluminum disc what may cause local overheating and disc deformation. More brushes on the disc periphery can prevent this phenomenon.
- The proposed construction of the motor allows one rotor disc to rotate in direction opposite to the rotation of other rotor disc. This can be done by reversing the current flow in one of the aluminum discs.

- A possibility of rotation of two rotor discs in opposite directions makes this motor attractive to the ship propulsion application.

6.2 Future Work

Due to the low efficiency at rated speed, a further study should concentrate on modification of the aluminum disc supply. One of the options is to add more brushes around disc circumference to make the current more radially oriented. Another task in future research is to build the physical motor model. It can be done by modifying the presently available disc homopolar motor model shown in figure 5.12.

REFERENCES

- [1] Michael Faraday, *New Electro-Magnetic Apparatus*. Quarterly Journal of Science, Literature and the Arts, Vol. XII, 1821: p.186-187
- [2] Emile Alglave & J.Boulard, *The Electric Light: It's History, Production, and Application*, translated by T.O'Conor Sloan, D.Appleton & Co., New York, 1884: p.224
- [3] Ernest Mendrela, "Introduction to homopolar DC motors" Lecture notes, Louisiana State University, Baton Rouge, LA
- [4] Jacek F.Gieras, *Superconducting Electrical Machines - State of the Art*, Przegląd elektrotechniczny, R.85, 12/2009.
- [5] Piotr Paplicki, "Configurations of slotless permanent magnet motors with counter-rotating rotors for ship propulsion drives" Przegląd elektrotechniczny, R.83, 11/2007.
- [6] David Meeker, "Finite Element Method Magnetics – Version 4.0", User's Manual, January 8, 2006.
- [7] Ansoft Corporation, "Introduction to Scripting in Maxwell – Version 12", User's Manual February, 2008.
- [8] Matweb: Material Property Data. February 9, 2011. <http://www.matweb.com/index.aspx>
- [9] Pavani Gottipati, "Comparative study on double-rotor PM brushless motors with cylindrical and disc type slot-less stator" M.S. thesis, Louisiana State University, Baton Rouge, LA, August 2007.
- [10] Neelavardhan Mallepally, "Performance analysis of homopolar DC motor" Project report, Louisiana State University, Baton Rouge, LA, May 2010.

APPENDIX A: M-FILES FOR STEADY STATE CHARACTERISTIC OF TWIN-ROTOR HOMOPOLAR DC MOTOR

a) M-file for speed and current vs. load torque characteristics

```

V=0.231;           % supply voltage
Kt=5.535*10^-4;   % electromagnetic torque coefficient
Ke=1.155*10^-3;   % emf coefficient
B=0.002;          % friction coefficient
Ra=2.30*10^-6;    % armature resistance
ia=723:3344/100:3344; % armature current
wm=(V-Ra*ia)/Ke; % angular speed
Tem=Kt*ia;        % electromagnetic torque
Tout=Tem-B*wm;    % output torque

clf
figure(1)
plot(Tout,wm,Tout,ia*0.1, 'r');
xlabel('Torque [N*m]');
gtext('speed [rad/sec]'),gtext('current*10 [A]');
```

M-file for Pin, Pout and efficiency vs. load torque characteristics

```

V=0.231;           % supply voltage
Kt=5.535*10^-4;   % electromagnetic torque coefficient
Ke=1.155*10^-3;   % emf coefficient
B=0.002;          % friction coefficient
Ra=2.30*10^-6;    % armature resistance
ia=723:3344/100:3344; % armature current
wm=(V-Ra*ia)/Ke; % angular speed
Tem=Kt*ia;        % electromagnetic torque
Tout=Tem-B*wm;    % output torque
Pout=Tout.*wm;    % output power
Pin=V*ia;         % input power
Eff=Pout./Pin*100; % efficiency

clf
figure(1)
plot(Tout,Pin,Tout,Pout,'--',Tout,Eff*10, 'r');
xlabel('Torque [N*m]');
gtext('input power [W]'),gtext('output power [W]'),gtext('efficiency/10 [%]');
```

APPENDIX B: M-FILES FOR DYNAMIC CHARACTERISTICS OF TWIN-ROTOR HOMOPOLAR DC MOTOR

a) M-file for angular speed, electromagnetic torque, load torque and armature current vs. time characteristics

```
load Current C; load speed1 w;load Torque T; load Speed n;  
I=C';w=w';T=T';n=n';  
t=I(:,1);I=I(:,2);w=w(:,2); Tem=T(:,2);TL=T(:,3);n=n(:,2);  
CLF
```

```
figure(1),  
subplot(2,1,1),  
plot(t,w,'k'),xlabel('time [s]'),ylabel('Angular speed [rad/s]'),
```

```
subplot(2,1,2),  
plot(t,Tem,t,TL),  
xlabel('time [s]'),ylabel('Torque [Nm]'),  
gtext('TL [Nm]'),gtext('Tem [Nm]');
```

```
figure(2),  
plot(t,I),  
xlabel('time [s]'),ylabel('Armature current [A]'),
```

b) M-file for armature current and angular speed vs. time characteristics in supply voltage ramped start-up process

```
load Current C; load speed1 w;load Torque T; load Speed n;load voltage V;  
I=C';w=w';T=T';n=n';V=V';  
t=I(:,1);I=I(:,2);w=w(:,2); Tem=T(:,2);TL=T(:,3);n=n(:,2);V=V(:,2);  
CLF
```

```
figure(1),  
subplot(2,1,1),  
plot(t,I,t,V*10000,'k'),xlabel('time [s]'),grid  
gtext('Current [A]'),gtext('Supply voltage*10e-4 [V]');
```

```
subplot(2,1,2),plot(t,w,'k'),xlabel('time [s]'),  
ylabel('Angular speed [rad/s]'),grid,
```

VITA

Zhiwei Wang, son of Gengtian Wang and Guirong Mu, was born in Taiyuan, Shanxi province, P.R.China. He received his Bachelor of Engineering in Electrical Automatic Control Engineering degree from Taiyuan University of Technology in 2004. After he graduated, he took a job as an electrical engineer intern at the 13th China Metallurgical Construction Corporation. Then, he joined the Department of Engineering in McNeese State University in Lake Charles, Louisiana. He pursued his Master of Engineering in Electrical Engineer in 2008. He passed the Fundamental of Engineer Exam (FE) in October 2007 and registered as a member of E.I. Associate in Louisiana Engineering Society in September 2009. He joined the Department of Electrical and Computer Engineering at Louisiana State University in August 2009 in Ph.D program. He will be awarded the degree of Master of Science in Electrical Engineering in May 2011.